Original research

DYRK1B blockade promotes tumoricidal macrophage activity in pancreatic cancer

Anna Brichkina [1,2] Miriam Ems,[1] Roman Suezov,[1] Rajeev Singh,[1] Veronika Lutz,[3] Felix S R Picard,[3] Andrea Nist,[4] Thorsten Stiewe,[4,5] Johannes Graumann,[6,7] Michael Daude,[8] Wibke E Diederich,[8,9] Florian Finkernagel,[10] Ho-Ryun Chung,[11] Detlef K Bartsch,[12] Katrin Roth,[13] Corinna Keber,[14] Carsten Denkert,[14] Magdalena Huber,[3] Thomas M Gress,[15] Matthias Lauth [1]

ABSTRACT

Objective Highly malignant pancreatic ductal adenocarcinoma (PDAC) is characterised by an abundant immunosuppressive and fibrotic tumour microenvironment (TME). Future therapeutic attempts will therefore demand the targeting of tumours and stromal compartments in order to be effective. Here we investigate whether dual specificity and tyrosine phosphorylation-regulated kinase 1B (DYRK1B) fulfil these criteria and represent a promising anticancer target in PDAC.

Design We used transplantation and autochthonous mouse models of PDAC with either genetic *Dyrk1b* loss or pharmacological DYRK1B inhibition, respectively. Mechanistic interactions between tumour cells and macrophages were studied in direct or indirect co-culture experiments. Histological analyses used tissue microarrays from patients with PDAC. Additional methodological approaches included bulk mRNA sequencing (transcriptomics) and proteomics (secretomics).

Results We found that DYRK1B is mainly expressed by pancreatic epithelial cancer cells and modulates the influx and activity of TME-associated macrophages through effects on the cancer cells themselves as well as through the tumour secretome. Mechanistically, genetic ablation or pharmacological inhibition of DYRK1B strongly attracts tumoricidal macrophages and, in addition, downregulates the phagocytosis checkpoint and 'don't eat me' signal CD24 on cancer cells, resulting in enhanced tumour cell phagocytosis. Consequently, tumour cells lacking DYRK1B hardly expand in transplantation experiments, despite their rapid growth in culture. Furthermore, combining a small-molecule DYRK1B-directed therapy with mammalian target of rapamycin inhibition and conventional chemotherapy stalls the growth of established tumours and results in a significant extension of life span in a highly aggressive autochthonous model of PDAC.

Conclusion In light of DYRK inhibitors currently entering clinical phase testing, our data thus provide a novel and clinically translatable approach targeting both the cancer cell compartment and its microenvironment.

WHAT IS ALREADY KNOWN ON THIS TOPIC

⇒ Elevated dual specificity and tyrosine phosphorylation-regulated kinase 1B (DYRK1B) expression can be found in approximately 40% of patients with pancreatic cancer, with about 9% of patients displaying genomic amplification of *DYRK1B*, suggesting an oncogenic role for this kinase.

⇒ The best-established function of DYRK1B is the promotion of proliferative quiescence, which at first seems odd given its role as an oncogene.

⇒ All other functions ascribed to DYRK1B (eg, survival and DNA repair) are also intrinsic to cells.

WHAT THIS STUDY ADDS

⇒ This study extends the tumour cell-intrinsic functions of DYRK1B to the regulation of the tumour microenvironment, in particular the myeloid compartment.

⇒ DYRK1B excludes tumoricidal macrophages from tumour sites and thereby promotes cancer growth.

⇒ In addition, DYRK1B upregulates the myeloid checkpoint CD24 on cancer cells, directly protecting them from phagocytic attacks by macrophages.

⇒ In terms of a translational perspective, we outline a non-toxic combination therapy including inhibitors of DYRK1B and mammalian target of rapamycin together with chemotherapy, which significantly extends survival in an aggressive murine pancreatic ductal adenocarcinoma model.

INTRODUCTION

Pancreatic ductal adenocarcinoma (PDAC) is a lethal disease with a 5-year survival rate of merely 10%–11%.[1] Patients typically present with advanced or metastatic disease, making surgical removal impossible and highlighting the need for novel treatment options affecting established tumours.[2] With disease incidence expected to rise in the coming years,[3] quickly translatable results from preclinical studies are even more critical in order to improve patient outcomes in the near future. With respect to small-molecule inhibitors, promising strategies to serve this need are combination therapies or the repurposing of already-approved drugs or novel compounds already in clinical testing.

Single-cell transcriptomic profiling has shed light on the complex makeup of the disease-distinguishing

HOW THIS STUDY MIGHT AFFECT RESEARCH, PRACTICE OR POLICY

⇒ This study establishes DYRK1B as a hitherto unknown regulator of tumour innate immunology. Since DYRK1B acts on multiple layers controlling macrophages, it may play a previously unrecognised central role within the crosstalk between tumour cells and tumour-associated macrophages.

⇒ Small-molecule DYRK1 inhibitors are currently in clinical testing, potentially allowing for a very timely translation of our findings to patients with pancreatic cancer.

tumour microenvironment (TME) and its adaptive behaviour to therapy.[4] Specifically, PDAC is characterised by a potent immunosuppressive TME, typically excluding cytotoxic T cells from the tumour bed or driving them into functional exhaustion.[5 6] Innate immunity, on the other hand, is abundant in the form of tumour-associated neutrophils (TANs) and tumour-associated macrophages (TAMs), thought to provide a potent immunosuppressive environment. Recent work has elucidated that the protumorigenic functionality of TAMs is also associated with their cell lineage, as PDAC harbours two subpopulations of TAMs: the embryonic yolk sac-derived macrophages and bone marrow-recruited monocytes or macrophages.[7] In the mouse, the former Ly6c^{low} cell subpopulation promotes fibrosis and PDAC progression, whereas the latter Ly6c^{high} subtype is enriched for major histocompatibility complex class II (*MHCII*) genes and antigen sampling, indicative of a benign or even tumour-suppressive phenotype.[7 8] The presence of the latter TAM population might also imply that clinical approaches could potentially benefit from a therapeutically induced recruitment of monocytes from the systemic circulation. Phenotypically, TAMs have traditionally been classified into a continuum of states ranging from the MHCII, CD80/86, interleukin (IL)12^{high} M1 state to a tumour-promoting MHCII^{low}, IL10^{high} M2 state.[9] Reprogramming procancerous cells into tumoricidal TAMs has therefore been of intense interest, as evidenced by the development of, for example, CD40 agonistic antibodies activating antigen-presenting cells.[10] Moreover, current translational ambitions not only aim at reprogramming TAMs towards an M1-like state but also facilitate cancer cell recognition by TAMs through antagonising endogenous innate immune checkpoints ('don't eat me' signals) such as CD47, CD24 or B2M, thus promoting cancer cell engulfment.[11 12]

The dual specificity and tyrosine phosphorylation-regulated kinases (DYRKs) belong to an understudied group of kinases with potential therapeutic impact (the so-called 'dark kinome'). This is particularly true for DYRK1B (a.k.a. MIRK),[13–15] which has been implicated in the aetiology of several malignancies where it regulates a multitude of oncogenic traits.[16–18] Despite DYRK1B behaving as an oncogene in many settings, it has also been described as a 'quiescence kinase' driving cell cycle exit in ovarian, colon and pancreatic cancer cells.[19–21] It is assumed that this function is crucial for resistance against chemotherapy and for disease relapse. Elevated *DYRK1B* messenger RNA (mRNA) expression can be detected in up to 40% of patients with pancreatic cancer and also in PDAC mouse models.[22] In approximately 9% of patients with PDAC, high DYRK1B protein levels are caused by genomic amplification of the *DYRK1B* gene.[17]

Here we show that DYRK1B promotes innate immune evasion and represents a promising drug target in PDAC. Although DYRK1B-depleted pancreatic cancer cells display enhanced cell proliferation in vitro, they are unable to support substantial tumour growth in vivo. Mechanistically, we could demonstrate that DYRK1B impacts the cancer cell secretome and profoundly regulates the immune TME. Here, DYRK1B acts on two levels of innate immune evasion. First, this kinase upregulates the surface expression of the self-recognition antigen CD24, protecting cancer cells from attack by phagocytic myeloid cells. Second, DYRK1B excludes macrophages from the tumour, and inhibition of DYRK1B not only results in massive recruitment of tumoricidal myeloid cells to the tumour bed but also increases the levels of phagocytosis of cancer cells and the enrichment of macrophage-activating Th1 cells. Based on these findings and on earlier work on a DYRK1B-mammalian target of rapamycin (mTOR) crosstalk,[16 18 23] we trialled a well-tolerated drug combination therapy and found it to significantly extend the survival of animals harbouring highly aggressive autochthonous PDAC by more than twofold. As DYRK inhibitors are currently entering phase I evaluation, our data open new possibilities for timely clinical targeting of critical tumour–stroma interactions.

MATERIALS AND METHODS

Cell lines

Mouse pancreatic adenocarcinoma cell lines (named mKpc) were derived from a spontaneous Kras$^{G12D/+}$, Trp53$^{R172H/+}$ and Pdx1-Cre (KPC) tumour. The presence of the expected mutations in *Kras* and *Trp53* was verified by Sanger sequencing of PCR-amplified complementary DNAs (cDNA). Immortalised mouse pancreatic stellate cell (mPSC) lines were kindly provided by Albrecht Neesse.[24] Human PSC1 (hPSC) cells were a kind gift of Matthias Löhr[25]; hPSC2 were kindly provided by Rosa Hwang.[26] The Panc1 and AsPC-1 cell lines were purchased from Cell Line Service (CLS, Germany); MiaPaca-2 and PA-TU-8988T cells were obtained from DSMZ (Germany). BxPC-3 and SU86.86 cells were purchased from ATCC. All cell lines were cultured in Dulbecco's Modified Eagle Medium (DMEM (high glucose plus glutamine and pyruvate), Invitrogen), supplemented with 10% foetal bovine serum (FBS; Anprotech, Germany) and 1% penicillin/streptomycin at 37°C with 5% carbon dioxide (CO$_2$). All cells were regularly checked for mycoplasma contamination.

Chemical compounds

AZ191 was synthesised in-house according to a published protocol.[27] KU0063794 was purchased from MedChemExpress MCE/MedChem Tronica and Everolimus from Biomol. Dimethyl sulfoxide (DMSO) was obtained from VWR or Applichem.

Generation of DYRK1B-KO/KD cell lines

The knockouts (KOs) of *Dyrk1b* in mKpc4 cells were generated according to a procedure described previously.[24] For targeting murine *Dyrk1b*, we used a pU6-Cas9-based plasmid backbone (Addgene #64324) harbouring the following 20 bp guide sequences: CRISPR2-CGGGGCAGGAGCCGCACATC (targets exon 3 of isoform c) and CRISPR5-CTATGCGAAGAAGAAG-CGGC (targets exon 4 of isoform c). Individual clones were harvested and screened for loss of DYRK1B in western blotting (WB), yielding clones 2.7 (CRISPR2) and 5.3 (CRISPR5). For human *DYRK1B*-knockdown (KD) generation, Panc1 cells were transfected with pLKO.1-puro plasmids containing one of the following targeting sequences (5'->3'): shCon-CAACAAGA TGAAGAGCACCAA (non-targeting control), sh*DYRK1B*_1-GACCTACAAGCACATCAATGA; sh*DYRK1B*_3- CACGGAGA TGAAGTACTATAT. Two days post-transfection, cells were treated with puromycin (2 μg/mL) until single clones appeared, which were subsequently picked, expanded and screened by WB.

Colony assays

Wild-type (WT) and KO mKpc4 cells were plated at a density of 500 cells per well in a six-well plate in DMEM supplemented with 1% penicillin/streptomycin and 10% FBS. After 2 days, cells were washed with Dulbecco's phosphate-buffered saline (DPBS) and cultured for 6–8 days in 0.5% FBS-containing medium. Subsequently, cells were washed with DPBS and trypsinised, counted or stained with a crystal violet solution (0.2% crystal violet, 10% ethanol (EtOH) and 5% methanol (MeOH)) followed by several washing steps with water to remove excess staining solution. Afterwards, culture plates were air-dried and scanned, and the number of visible colonies was counted. For colony formation in the presence of drugs, the growth medium was supplemented with 0.2 µM KU0063794 or 0.2 µM Everolimus, and control cells received the solvent DMSO.

Bromodeoxyuridine (BrDU) staining

mKpc4 cells plated on six-well plates were serum-starved (0.5% FBS in DMEM) for 2 days, and 10 µM BrDU (Sigma) was added to the growing cells for 4 hours. Cells were trypsinised and harvested by centrifugation at 300g for 5 min. The cell pellet was resuspended in 200 µL of ice-cold DPBS, and 500 µL of ice-cold 70% EtOH was slowly added while the cells were vortexed. After fixation for 30 min on ice, cells were pelleted by centrifugation at 300g for 5 min. The cell pellet was resuspended in 500 µL of 2 M hydrochloric acid containing 0.5% Triton X-100 while vortexing. After incubation at room temperature (RT) for 30 min, the cells were centrifuged at 8000 rpm for 2 min. The cell pellet was resuspended in 500 µL of 0.1 M sodium borate (pH 8.5) to neutralise the acid and centrifuged at 8000 rpm for 2 min. Cells were stained for 30 min at RT in 150 µL of DPBS containing 1% bovine serum albumin (BSA)/0.5% Tween-20 and supplemented with 8 µL of anti-BrDU fluorescein isothiocyanate antibodies (BD Bioscience). Cells were washed once with DPBS containing 1% BSA/0.05% Tween 20, centrifuged and resuspended in 500 µL of DPBS with 1 µg/mL of propidium iodide and analysed by Cytoflex LX Series (Beckman Coulter, USA).

RNA/cDNA/quantitative reverse transcription (qRT)-PCR analysis

Total RNA was extracted using the NucleoSpin RNA II kit from Macherey-Nagel according to the manufacturer's protocol. 0.5–1 µg of total RNA was used for cDNA synthesis performed with the iScript cDNA Synthesis Kit (BioRad). For quantitative PCR (qPCR) reactions, the Absolute QPCR SYBR Green Mix (Thermo Scientific) was used. qPCR reactions were performed on 96-well plates using the Mx3005P qPCR systems (Agilent). Relative expression was calculated according to the $2^{\Delta\Delta Ct}$ method. For specific information on qPCR primer sequences, please refer to online supplemental file.

RNAseq

Cellular RNA was extracted using the Macherey-Nagel NucleoSpin RNA Isolation Kit, according to the manufacturer's protocol. The integrity of the total RNA was assessed by capillary electrophoresis. RNAseq libraries were generated using Lexogen Quantseq according to the manufacturer's protocol and sequenced on an Illumina NextSeq 550 using 75 bp single-end reads. Raw reads were aligned to the human genome (GRCh38) using STAR V.2.6.1d and quantified as counts per million against the protein-coding and lincRNA-coding genes as defined by Ensembl,[28] revision 100. Statistical comparisons were performed via unpaired DESeq2.[29] Functional annotation was performed with hypergometrical tests and Benjamini-Hochberg correction versus the Molecular Signatures Database.

Western blotting

Cells were lysed in 1× sample buffer; separation of lysates by sodium dodecyl sulphate polyacrylamide gel electrophoresis (Bio-Rad) and subsequent blotting on Immobilon-polyvinylidene difluoride membranes (Millipore) was done as described in Schneider et al,[30] followed by incubation with the respective primary antibody. After incubation with a corresponding horseradish peroxidase (HRP)-coupled secondary antibody (Cell Signalling Technology), the HRP signal was detected using Pierce ECL Western Blotting Substrate (Thermo Scientific) according to the manufacturer's protocol. For specific antibodies, see online supplemental file.

Isolation and differentiation of mouse bone-marrow-derived macrophages (BMDM)

Bone marrow was collected from the femur bones of C57Bl/6 mice by flushing with Roswell Park Memorial Institute Medium (RPMI)-1640 medium containing 1% penicillin/streptomycin and passing through a 70-micron cell filter. The cell suspension was centrifuged at 300g for 5 min, and the cell pellet was incubated in erythrocyte lysis buffer (155 mM ammonium chloride, 12 mM sodium bicarbonate and 0.1 mM EDTA) for 3 min at RT, followed by centrifugation at 300g for 5 min. Bone marrow cells were plated on a six-well plate and cultured in RPMI-1640 medium (with glutamine and pyruvate) supplemented with 10% FBS, 1% penicillin/streptomycin and 20 ng/mL of recombinant macrophage colony-stimulating factor (Immunotools, Germany). Cells were incubated for 4–5 days at 37°C in a humid atmosphere containing 5% CO_2 to allow differentiation into macrophages.

Isolation of human peripheral blood mononuclear cells (PBMC) and differentiation into macrophages

Chambers of the leucoreduction system with blood from healthy adult volunteers were provided by the Center for Transfusion Medicine and Hemotherapy at the University Hospital Giessen and Marburg. Blood was carefully layered on 15 mL Ficoll (Capricorn Scientific, Germany), and the tube was centrifuged at 1080g for 20 min at RT (without break). After centrifugation, mononuclear cells were collected, resuspended in 40 mL of DPBS and centrifuged at 300g for 5 min at RT. The cell pellet was resuspended in 40 mL of DPBS and centrifuged again at 10g for 10 min at RT. Pelleted cells were resuspended in 10 mL of DPBS, counted and plated as follows: 3×10^6 cells per well in a six-well plate or 0.7×10^6 per well in a 24-well plate. Plated cells were cultivated in DPBS for 30 min in an incubator at 37°C in a humid atmosphere with 5% CO_2 to enrich for monocytes. Attached cells were washed twice with DPBS to remove poorly attached cells and grown in RPMI-1640 medium supplemented with 5% human serum (Sigma, Germany), 1% penicillin/streptomycin, 2 mM GlutaMAX and 1 mM sodium pyruvate (Sigma) for 8 days at 37°C in a humid atmosphere containing 5% CO_2 to allow differentiation into macrophages. Subsequently, differentiated macrophages were washed twice with DPBS and subjected to treatments with supernatant (SN) from human pancreatic cancer cells or used to evaluate phagocytic capability.

Collections of SN from tumour cells and macrophages

For SN production, mKpc4 cells were plated at a density of 2×10^5 cells per 10 cm culture dish and Panc1 cells at a density

of 4×10^5 cells per 10 cm dish in DMEM supplemented with 1% penicillin/streptomycin and 10% FBS. Two days later, cells were washed with DPBS and the medium was replaced with 0.5% FBS-containing DMEM. Two days later, conditioned media (SN) was collected, centrifuged at 300*g* for 5 min to deplete cell debris and frozen at −80°C.

To collect conditioned media from macrophages, BMDM were differentiated for 5 days, washed twice with DPBS, treated with SN from mKpc4 cells in a ratio of 1:2 (1/3 volume of SN) and incubated for 24 hours. Control macrophages were incubated with the same proportion of medium containing 0.5% FBS. The next day, the cells were washed with DPBS and either lysed for further purification of total RNA or incubated with DMEM medium containing 2% FBS and 1% penicillin/streptomycin for an additional 72 hours. At this point, macrophages were counted and the conditioned medium was harvested, centrifuged at 300*g* for 5 min and frozen at −80°C for further analysis.

Human PBMC-derived macrophages were differentiated for 8 days, washed twice with DPBS, treated with SN collected from Panc1 cells in a ratio of 1:2 (1/3 volume of SN) and incubated for 24 hours. Control macrophages were incubated with the same proportion of medium containing 0.5% FBS. The next day, the cells were washed with DPBS and lysed for the purification of total RNA.

Allograft experiment
Mice were kept under specified pathogen-free (SPF) conditions in individually ventilated cages with a 12 hour/12 hour light–dark cycle and a standard altromin housing diet. For the experiment, female C57BL/6 mice were randomly divided into two groups (3–5 animals per cage). 1×10^5 WT or *Dyrk1b*-KO (clone 5.3) mKpc4 cells were suspended in a total volume of 150 µL of DMEM medium. The cell suspensions were injected subcutaneously at the posterior flank of the mice. The size of the tumours was measured two times per week using a calliper. Tumour volumes were calculated by the formula (length×width^2)/2. The length represents the longer axis and the width represents the shorter axis of the tumour. At the experimental endpoint, mice were euthanised and tumours were removed. The study was approved by the regional agency on animal experimentation (Regierungspräsidium Giessen).

KPC mouse model and drug treatment
Mice were kept under SPF conditions in individually ventilated cages with a 12 hour/12 hour light–dark cycle and a standard altromin housing diet. To obtain KPC mice, LSL-Kras$^{G12D/+}$ and LSL-Trp53$^{R172H/+}$ mice were crossed with Pdx1-Cre mice, yielding triple-mutant mice: LSL-Kras$^{G12D/+}$, LSL-Trp53$^{R172H/+}$ and Pdx1-Cre (KPC). KPC animals of both sexes underwent weekly abdominal palpation starting at the age of 10 weeks. Once a tumour was identified by palpation, a small animal ultrasound was performed to measure its size. Pharmacological treatment was initiated when tumour size reached about 100–150 mm^3, calculated by the formula (length×width^2)/2. The length represents the longer axis and the width represents the shorter axis of the tumour. Gemcitabine (70 mg/kg; once weekly), AZ191 (5 mg/kg; two times per week) and KU0063794 (5 mg/kg; two times per week) were dissolved in 50% 2-hydroxypropyl-β-cyclodextran (Sigma)/DPBS and injected intraperitoneally. The control group received equal volumes of solvent. Tumour sizes were regularly determined by ultrasound until the animal had to be sacrificed. All studies were approved by the regional agency on animal experimentation (Regierungspräsidium Giessen).

Culture of murine PSCs in a three-dimensional (3D) matrix
PSCs (mPSC4, kindly obtained from Dr Albrecht Neesse) were seeded at a density of 6×10^5 in a 70 µL matrigel drop containing a 1:1 ratio of DMEM (10% FBS) and growth factor-reduced basement membrane matrix (Corning, Cat #356230) on a 3.5 cm suspension dish (Sarstedt). The matrigel-embedded mPSC4 was covered with 0.5% FBS-containing DMEM and incubated for 48 hours to obtain quiescent mPSC4 (qPSC). Thereafter, qPSC were incubated with 1/3 of the volume of SN from activated BMDM for 48 hours. After differentiation, qPCR-based phenotyping was performed. For this, medium was removed and drops were collected in ice-cold PBS and centrifuged at 1000 rpm for 5 min at 4°C. After removing PBS, Matrigel drops were intensively resuspended in ice-cold PBS and incubated for 30 min at 4°C. Cells were centrifuged (1000 rpm, 4°C, 5 min), and pellets were frozen at −80°C for later RNA preparation.

Immunohistochemistry
For immunohistochemistry of formalin-fixed paraffin-embedded (FFPE) tissue, heat-induced epitope retrieval was performed with EDTA. Staining was performed on a DAKO Autostainer-Plus. After blocking endogenous peroxidases, sections were incubated for 45 min with the respective antibody. Sections were washed and incubated with Dako REAL EnVision HRP Rabbit/Mouse polymer, which reacts with DAB-Chromogen, according to the manufacturer's protocol. The use of patient material (in the form of tissue microarrays) was approved by the local ethics committee (Ethics Board University Hospital Marburg). The tissue used in this study was surgically resected primary tumour material obtained from patients with PDAC eligible for surgery.

Immunofluorescence (IF) of FFPE tissue and image analysis
For IF using fluorophore-conjugated antibodies, antigen retrieval of tissue sections was achieved by steam-heating in citrate solution (pH 6.0, Mophisto) for 30 min. Sections were then treated with 100 mM glycine for 10 min, washed with Tris-buffered saline with 0.1% Tween 20 detergent (TBS-T) and blocked with 10% goat serum in PBS containing 0.3% Triton for 60 min. Subsequently, sections were incubated overnight at 4°C with primary antibodies diluted in PBS supplemented with 5% goat serum and 0.3% Triton X100. After washing with TBS-T, samples were incubated with corresponding secondary antibodies for 60 min at RT, followed by washing and mounting.

The analysis of the images was done with Imaris 9.9.0 (Oxford Instruments). Macrophages were detected by the spot algorithm. The same was done for CD206 and tumour necrosis factor (TNF). For the analysis of CD206$^+$ macrophages and TNF$^+$ macrophages, the number of double-positive cells in all macrophages was determined. For Ki67, the surface algorithm was chosen, and the colocalized part of macrophages was counted. Pan-cytokeratin was also determined by the surface algorithm. In addition, the classification of the surfaces was selected to distinguish between surfaces with the shortest distance to Ki67 positive surfaces below 1 µm (Ki67$^+$Cytokeratin$^+$ cells) and Ki67$^-$cytokeratin$^+$ cells.

Phagocytosis assay
Human or mouse macrophages were plated on a 24-well plate and differentiated according to the protocol described above. After differentiation, macrophages were either treated for 24 hours with 1/3 volume of conditioned media from corresponding tumour cells or proceeded directly to the phagocytosis assay. One well of macrophages was used to count cells. Plated

macrophages were stained for 20 min with CellTracker Green CMFDA (Invitrogen) diluted in plain RPMI medium according to the manufacturer's instructions. Tumour cells were harvested, counted and an equal number (compared with macrophages) of tumour cells (mKpc4 or Panc1) were stained with CellTracker Deep Red (Invitrogen) diluted in plain RPMI according to the manufacturer's instructions. Macrophages and tumour cells were washed with DPBS, and an equal number of tumour cells were plated into each well with macrophages. Single stained and unstained cells were also preserved as samples for gating. 14–18 hours later (overnight), cells from wells were trypsinised, harvested, resuspended in 200 μL of DPBS containing 1% BSA and 2 mM EDTA and fixed by the addition of 200 μL 4% paraformaldehyde. Unstained, single-only stained and mixed cells were analysed by flow cytometry using the Cytoflex LX Series (Beckman Coulter).

Macrophage migration

Each bottom of a well of a 24-well plate was loaded with 500 μL of SN from corresponding tumour cells and 500 μL of 0.5% FBS-containing DMEM. Control wells received 1 mL of 0.5% FBS-containing DMEM. Differentiated mouse or human macrophages were trypsinised and counted. Counted macrophages were centrifuged at 300g for 5 min, and the pellet was resuspended in DMEM containing 0.5% FBS. A 500-μL cell suspension with 1×10^5 macrophages was loaded onto a tissue culture insert with a pore diameter of 8 μM (Sarstedt). 24 hours later, media were aspirated, and cells were washed with DPBS. Cells on the upper surface of the insert were removed by a cotton bud, whereas cells from the bottom surface were stained with a crystal violet solution (0.2% crystal violet, 10% EtOH and 5% MetOH) for 2 hours. Subsequently, inserts were intensively washed with distilled water and air-dried. Inserts with stained cells were placed in a new 24-well plate containing 20% acetic acid in water, incubated on a shaker for 30 min, and the absorbance of the coloured solution was measured at 590 nm using an MWG-Biotech SpectraMax340 spectrophotometer.

Viability assay

Mouse BMDM were differentiated for 5 days and treated for 24 hours with 1/3 volume of SN from corresponding tumour cells. Control wells were treated with 1/3 volume of 0.5% FBS-containing DMEM medium. On the next day, macrophages were washed with PBS and cultivated for an additional 3 days in DMEM containing 0.5% FBS and counted using Neubauer counting chambers.

Surface staining of CD24

mKpc4 and Panc1 cells were trypsinised, harvested and counted. Then, 5×10^5 cells were resuspended in 100 μL of DPBS containing 1% BSA and antibodies blocking Fc-receptors (Miltenyi, Germany). After incubation for 10 min at RT, 1 μL of phycoerythrin (PE)-conjugated anti-CD24 antibodies (Biolegend) or PE-conjugated isotype control IgG (Biolegend) was added to the tube, and cells were stained for 15 min at 4°C. Cells were washed twice with DPBS containing 1% BSA and 2 mM EDTA and were then analysed using the Cytoflex LX Series (Beckman Coulter). The data were analysed using FlowJo software.

Flow cytometry of mouse tumours

After surgical removal, tumours were digested into single-cell solutions by 200 u/mL Collagenase IV (Worthington), 10 μg/ mL DNAse I (Roche) in Hanks' balanced salt solution, 37°C, 300 rpm agitation and filtered through 100-μm cell strainers (Sysmex). Subsequently, staining with fluorophore-conjugated antibodies was performed. The flow profiles were acquired on an Attune NxT Cytometer (Thermofisher Scientific) or a Cytoflex LX Series (Beckman Coulter).

Cytokine array

Conditioned media (SN) was collected as described above from parental mKpc4 cells and *Dyrk1b*-KO clone 5.3. Conditioned media was diluted with the provided dilution buffer 1:2 (1/3 volume of SN) and subjected to secretome analysis using the mouse XL cytokine array kit (R&D Systems, USA) according to the manufacturer's instructions.

Soft agar colony formation assay

Prewarmed sterile 5% Bacto-Agar (Roth, Germany) was mixed 1:10 with warm DMEM containing 10% FBS and loaded on wells of a six-well plate to solidify. 1×10^4 WT/KO mKpc4 cells were resuspended in 250 μL of warm DMEM containing 10% FBS and mixed with 500 μL of warm agar prediluted as above.

Cells resuspended in agar were loaded on top of solidified agar and grown for 10 days. Formed colonies were counted using a light microscope.

Secretome proteomics

4×10^5 WT/KO mKpc4 cells were plated on 6 cm dishes in independent triplicates in DMEM containing 10% FBS. Two days later, cells were washed with DPBS, and the medium was changed to DMEM without serum. Conditioned medium was collected after 2 days, centrifuged at 300g for 5 min to deplete debris and snap-frozen in liquid nitrogen for further proteomics studies. Modifying a protocol by Chevallet *et al*,[31] proteins were precipitated after the addition of cOmplete ULTRA Protease Inhibitor Cocktail without EDTA (Roche) as follows: in polypropylene tubes, samples were adjusted to final concentrations of 0.1% and 7.5% of *N*-lauroylsarcosine sodium salt and trichloroacetic acid, respectively, followed by incubation on ice for 2 hours and centrifugation at 10000g for 10 min at 4°C. Protein pellets were washed twice using cold tetrahydrofuran (10% initial sample volume) and stored at −20°C. Further sample processing included solution digest, reductive dimethyl labelling and high pH reverse phase chromatographic separation as described, followed by liquid chromatography-tandem mass spectrometric analysis on a Q Exactive HF mass spectrometer as described.[32 33] The MaxQuant suite of algorithms (V.2.0.1.0)[34] was used to analyse mass spectrometric raw data against the murine Uniprot database (canonical and isoforms; downloaded 2021/02/08_8661807 entries). False discovery rates of 1% were used both at the peptide and the protein group levels. Instrument parametrisation was extracted and summarised using MARMoSET[35] and along with the MaxQuant settings and mass spectrometric raw data, it has been deposited with the proteomeXchange consortium via the MASSive repository. The in-house R pipeline autonomics https://doi.org/doi:10.18129/B9.bioc.autonomics was used for downstream bioinformatic analysis.

Patient involvement

Tissue samples of patients with therapy-naive PDAC who underwent surgical resection were provided by the Biobank of the University of Marburg (CBBMR) in accordance with the regulations of the ethics committee of the University of Marburg (AZ 76–17).

Statistics and data accessibility

Statistical comparisons were made of n≥3 experiments using an unpaired two-tailed one-grouped Student's t-test (using MS Excel or GraphPad Prism) unless otherwise indicated. Significances were indicated as ns (not significant; $p>0.05$), $*p<0.05$, $**p<0.01$ and $***p<0.001$. Human Kaplan-Meier curves from public datasets were generated using the R2: Genomics Analysis and Visualisation Platform (http://r2.amc.nl). RNAseq data has been deposited at BioStudies/Array Express with the following accession codes: E-MTAB-13666 (*Dyrk1b* WT/KO in mKpc4 cells); E-MTAB-13667 (mouse allograft with *Dyrk1b* WT/KO mKpc4 cells) and E-MTAB-13668 (mouse BMDMs treated with SN from *Dyrk1b* WT/KO mKpc4 cells). Protein mass spectrometric raw data has been deposited with the proteomeXchange consortium via the MASSive repository.

RESULTS

The DYRK1B kinase is enriched in PDAC tumour cells

The DYRK1B kinase can be detected in 12%–39% of all PDAC cases, and in 6%–9%, this is caused by a genomic amplicon encompassing the *DYRK1B* gene locus (online supplemental figure S1A).[17 36] In order to validate these findings, we commenced our studies on DYRK1B in pancreatic cancer by first determining *DYRK1B* mRNA expression levels in bulk PDAC resection material (Marburg cohort; n=59 patients). As evident from figure 1A, *DYRK1B* mRNA levels were low but readily detectable and were significantly increased in the basal versus the classical subtype of PDAC (figure 1A). In patients with pancreatic cancer, high *DYRK1B* expression was associated with poorer overall survival compared with low-expressing patients (figure 1B; Yeh cohort; n=102[37]), a finding that was validated in an independent second public data set (online supplemental figure S1B; The Cancer Genome Atlas (TCGA) cohort; n=146 patients). Analysis of a recent scRNAseq study[38] revealed *DYRK1B* transcript expression to be primarily confined to epithelial duct cells of the pancreas as well as, to a lesser extent, endothelial and endocrine cells, but not acinar, stellate or immune cells (online supplemental figure S1C,D). In agreement with this observation, DYRK1B protein expression was observed in several human PDAC cell lines, but levels were low in PSCs (figure 1C). In addition, immunohistochemistry of human PDAC tissue supported these results, with DYRK1B being preferentially enriched in the epithelial tumour compartment (figure 1D). In the mouse, *Dyrk1b* mRNA expression can readily be measured in bulk tissue derived from the well-established KPC model of PDAC[39] as well as in epithelial cell-enriched tumour organoids (figure 1E). As shown for the human cell lines above, immunoblotting detected prominent DYRK1B protein levels in murine PDAC cell lines but only in marginal levels in mouse PSCs (figure 1F). Finally, mouse KPC tissue staining with a DYRK1B-specific antibody revealed clear enrichment of this kinase in the epithelial tumour compartment with only minute signals in the surrounding stroma (figure 1G and online supplemental figure S1E for antibody validation). Taken together, we could provide evidence that DYRK1B expression is preferentially restricted to tumour cells (and not the stroma) and negatively associated with overall survival in patients with PDAC.

DYRK1B suppresses PDAC cell proliferation in an mTOR-dependent manner

In order to shed more light on the precise role of DYRK1B in pancreatic cancer, we generated CRISPR/Cas9-mediated gene KO in murine PDAC cells (mKpc4) derived from the KPC mouse model[39] harbouring mutant $Kras^{G12D}$ and $p53^{R172H}$. Using two different CRISPR constructs targeting separate exons of the *Dyrk1b* gene, we identified two clones displaying complete (KO5.3) or almost complete (KO2.7) elimination of the DYRK1B protein (figure 2A), with no apparent changes in levels of the closely related paralogue DYRK1A (online supplemental figure S2A). In line with DYRK1B negatively regulating cell cycle components[20 40] and the DREAM (DP, RB-like, E2F And MuvB) complex,[41] *Dyrk1b*-KO cells grew significantly faster in culture than WT cells (figure 2B,C). Similar results were obtained in 3D culture using soft agar conditions (online supplemental figure S2B). KO cells displayed a higher rate of BrDU incorporation, showing that the increase in cell numbers was primarily caused by a faster cell cycle and not by enhanced survival (figure 2D and online supplemental figure S2C). Similar elevated incorporation was also observed upon treatment of *Dyrk1b*-WT cells with the small molecule DYRK1B inhibitor AZ191[42] (figure 2E and S2D). In addition, *Dyrk1b*-depleted cells were particularly sensitive to inhibition of the pro-proliferative mTOR kinase by either Everolimus (mTORC1 inhibitor) or KU0063794 (dual mTORC1/2 inhibitor), completely abrogating the surplus in proliferation seen upon *Dyrk1b* loss (figure 2F,G). In agreement with the increased sensitivity against mTOR inhibition, KO cells displayed stronger mTOR and S6 activation compared with WT cells (online supplemental figure S2E).

Intriguingly, transcriptome analysis revealed an upregulation of transforming growth factor β (TGFβ)-related gene signatures in *Dyrk1b*-KO cells (figure 2H), which were validated using qRT-PCR (figure 2I). In addition, the morphology of both KO clones appeared more mesenchymal as compared with their *Dyrk1b* WT counterparts (figure 2J). In summary, we could show that loss of *Dyrk1b* results in the induction of TGFβ pathway genes and mTOR-dependent stimulation of proliferation in pancreatic cancer cells.

Ablation of tumour cell-*Dyrk1b* stimulates macrophage recruitment

In light of the cell cycle-suppressive impact of DYRK1B in cultured cells, we were interested to investigate the corresponding outcome of *Dyrk1b* loss in an in vivo setting. To this end, we subcutaneously transplanted *Dyrk1b* WT or KO mouse PDAC cells into syngeneic C57BL/6 animals (figure 3A). In complete contrast to the cell culture experiments described above, KO cells were significantly growth retarded in this setting and only formed very small tumours, whereas WT cells gave rise to large tumours (figure 3B). Similar findings were also made with the second KO clone (online supplemental figure S3A). In order to obtain further insight into the underlying mechanisms, we performed mRNA sequencing (RNAseq) of bulk tumour tissues. Intriguingly, functional annotation of genes significantly upregulated in KO versus WT tumours yielded several innate immune signatures, such as interferon signalling, lipopolysaccharide, TNF, polyI:C-RNA or IRF3 (figure 3C), suggesting KO tumours to harbour an altered immune microenvironment compared with WT. Downregulated signatures included many general cancer terms (eg, nasopharyngeal carcinoma) as well as signatures associated with cellular differentiation (eg, breast cancer_luminal vs mesenchymal) (online supplemental figure S3B).

Following up on the observation of a potentially altered TME in the KO setting, we stained WT and KO tumour tissue with various antibodies detecting proliferation (Ki67), myofibroblastic cancer-associated fibroblasts (myCAFs; α-Smooth muscle actin
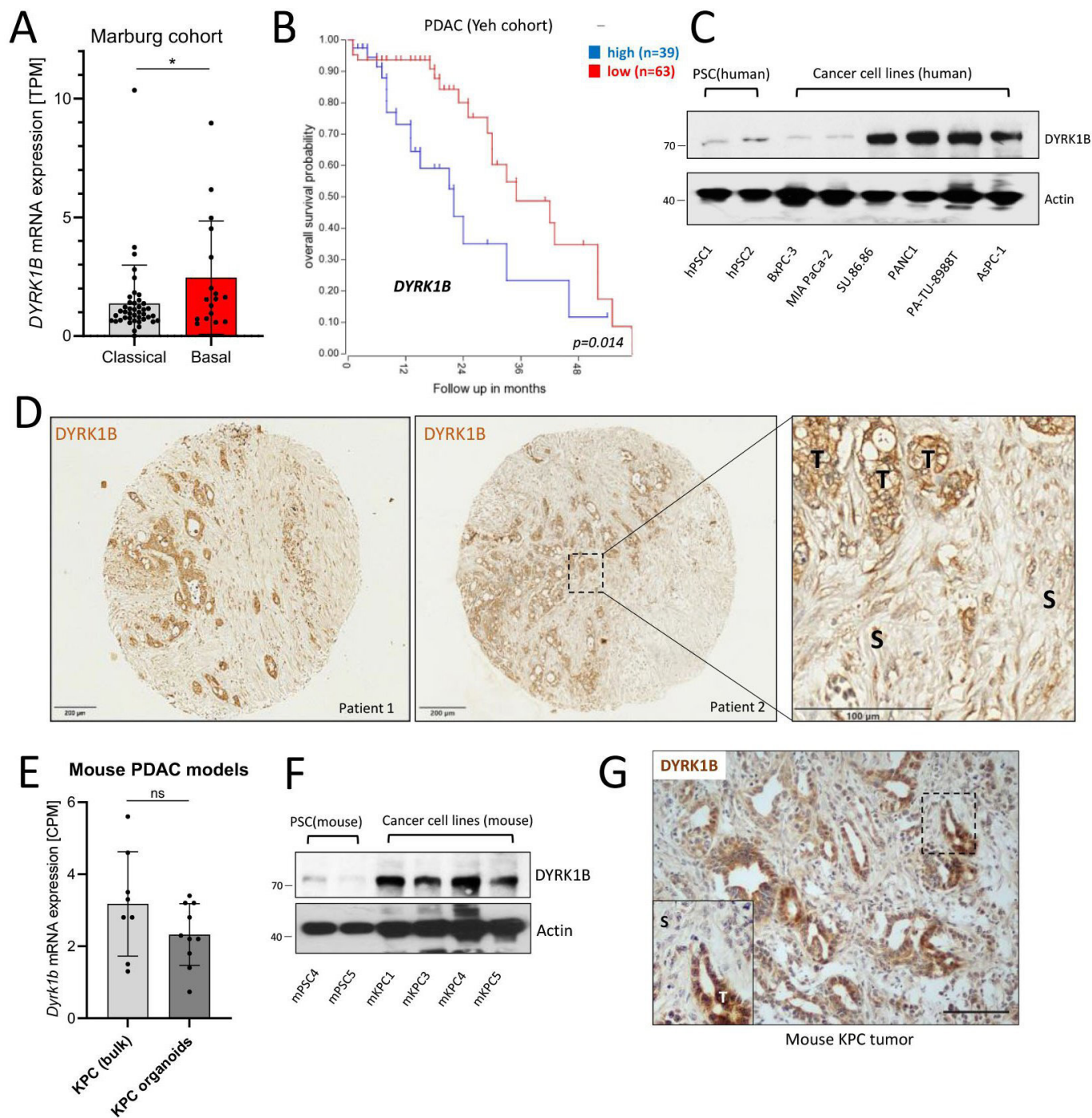
Figure 1 DYRK1B is expressed in pancreatic cancer cells. (A) *DYRK1B* mRNA expression (in transcript per million) in bulk tissue derived from patients with PDAC (n=59). Subtype classification as described in Rashid *et al.*[56] Each dot represents one patient (mean±SD). (B) Kaplan-Meier plot depicting overall survival of patients with PDAC[37] in relation to *DYRK1B* expression (Yeh cohort, scan split and log-rank test). (C) DYRK1B immunoblot of human cell lines. Actin was used as a loading control. Shown is one representative blot of n=2. (D) DYRK1B immunohistochemistry of tissue microarrays derived from resected PDAC material. (E) *Dyrk1b* mRNA expression (in counts per million) from mouse KPC bulk tissue and from KPC-derived primary organoids. Each dot represents one animal or one organoid line. (F) DYRK1B Western blot of murine cell lines. Shown is one representative blot of n=2. (G) DYRK1B immunohistochemistry on mouse KPC tumour tissue. The scale bar is 100 μm. DYRK1B, dual specificity and tyrosine phosphorylation-regulated kinase 1B; mRNA, messenger RNA; PDAC, pancreatic ductal adenocarcinoma; S, tumour stroma area; T, epithelial tumour area; TCGA, The Cancer Genome Atlas.

(α-SMA)), inflammatory CAFs (iCAFs; Platelet-derived growth factor receptor β (PDGFRβ)), vasculature (CD31) or tumour-associated macrophages (TAMs; F4/80) (figure 3D). Intriguingly, tumour cell proliferation as assessed by KI67 staining was unaffected in vivo, arguing that the microenvironment (and not

tumour cell-intrinsic proliferative alterations) was responsible for the observed growth retardation (figure 3E). Blood vessel density (CD31 staining) was moderate (figure 3F), while iCAF (PDGFRβ staining) abundance was profoundly reduced in KO tumours without significant changes in myCAFs (α-SMA)
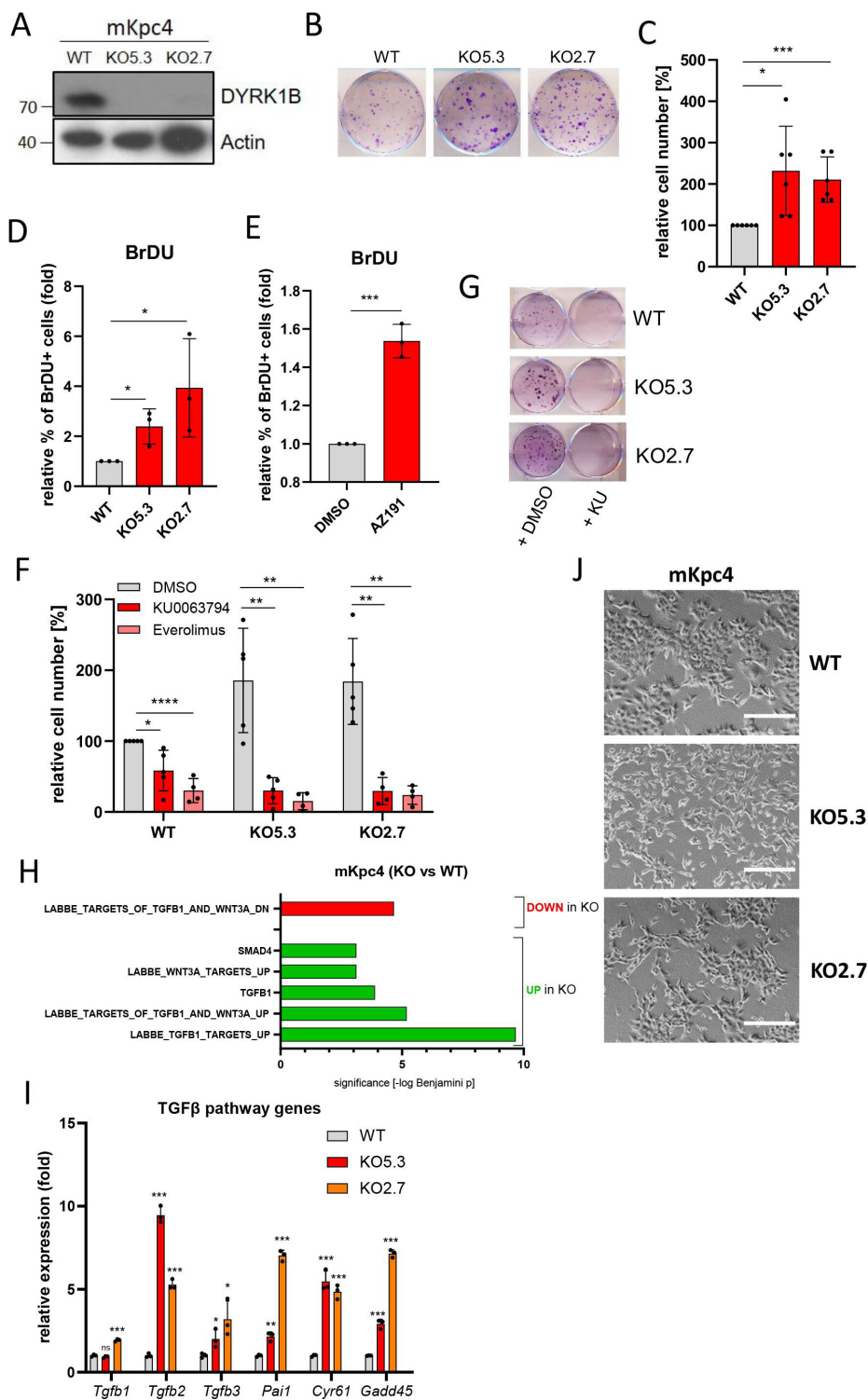
7

Figure 2 DYRK1B suppresses PDAC cell proliferation. (A) Western blot depicting DYRK1B protein levels in parental mKpc4 cells (WT) and DYRK1BKO clones 5.3 (KO5.3) and 2.7 (KO2.7). Actin was used as a loading control. Shown is one representative blot of n=3. (B) Colony staining (crystal violet, blue) of *Dyrk1b*-WT and *Dyrk1b*-KO mKpc4 clones. Shown is one representative of n=6. (C) Relative cell number (%) of mKpc4 cells grown in clonal density. Mean of n=6±SD (one-tailed t-test). (D) The relative percentage of BrDU-positive *Dyrk1b*-WT/KO mKpc4 cells. Mean of n=3±SD. (E) The relative percentage of BrDU-positive mKpc4 cells treated with DMSO as a solvent or 1 µM AZ191 for 4 days. Mean of n=3±SD. (F) Relative cell number (%) of WT/KO mKpc4 cells treated with solvent (DMSO) or 0.2 µM KU0063794 or 0.2 µM Everolimus for 6 days. Mean of n=4–5±SD. (G) Colony stain (crystal violet, blue) of WT/KO mKpc4 cells treated with solvent DMSO or 0.2 µM KU0063794. Shown is one representative of n=5. (H) Transcriptome signatures (RNAseq) of KO mKpc4 cells in comparison to WT cells. (I) Relative mRNA expression of TGFβ-pathway genes in WT and KO mKpc4 cells as determined by quantitative reverse transcription-PCR. Shown is one representative of n=3, measured in triplicate (±SD). Asterisks indicate significance versus WT. (J) Representative phase-contrast images of WT/KO mKpc4 cells. The scale bar is 50 µm. BrDU, bromodeoxyuridine; DMSO, dimethyl sulfoxide; DYRK1B, dual specificity and tyrosine phosphorylation-regulated kinase 1B; KO, knockout; mRNA, messenger RNA; PDAC, pancreatic ductal adenocarcinoma; TGFβ, transforming growth factor beta; WT, wild-type.
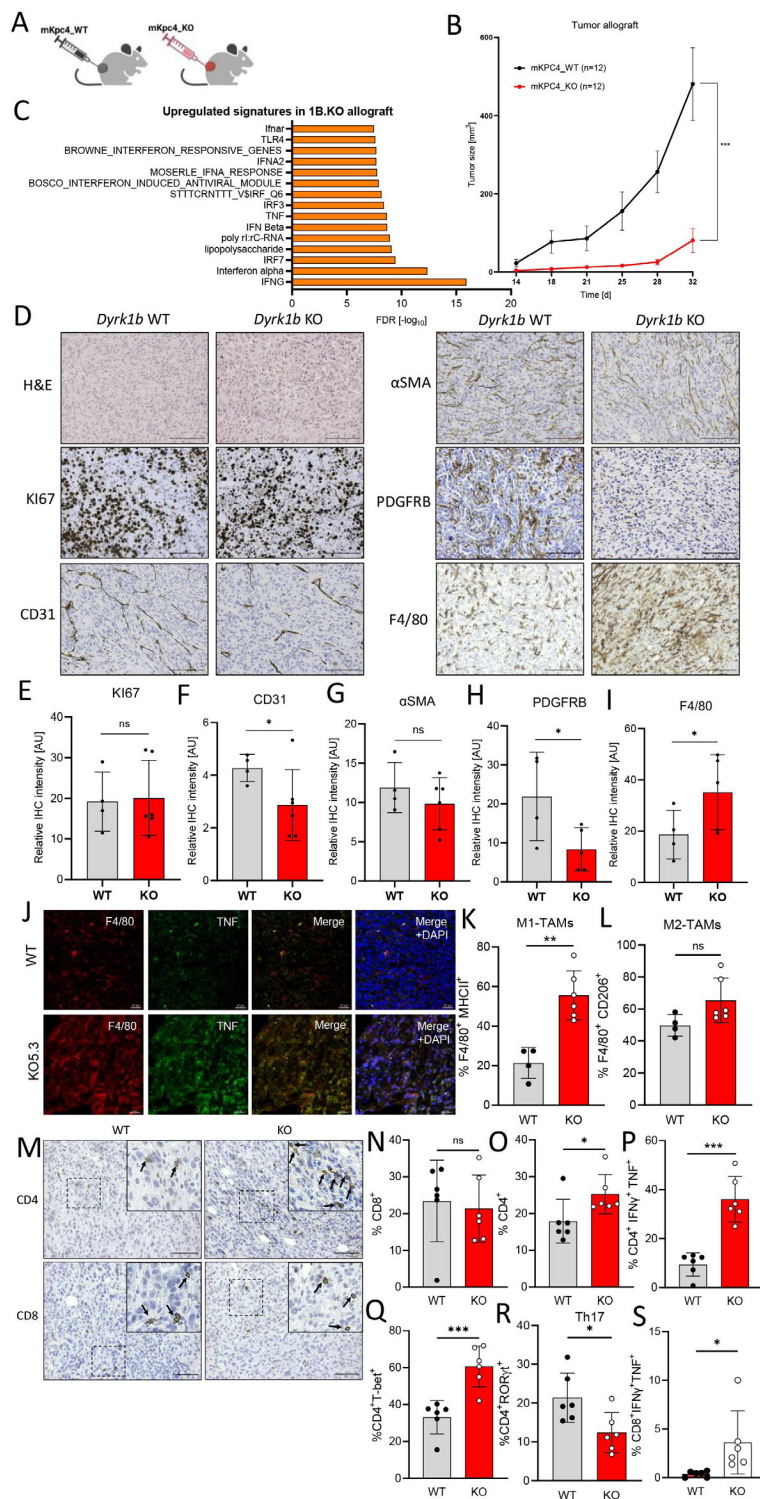
Figure 3 Ablation of tumour cell-*Dyrk1b* stimulates macrophage recruitment and inhibits in vivo tumour growth. (A) Scheme outlining the allograft experiment. (B) Tumour size changes over time (subcutaneous allograft growth in C57BL/6 mice). Animals received either *Dyrk1b*-WT (black curve) or KO (clone 5.3; red curve) mKpc4 cells (n=12 each) on day 0. Shown is the mean±SEM. (C) Gene signatures (RNAseq) upregulated in the KO allograft (vs WT). (D) Representative histology of resulting tumours from B. The upper panel depicts H&E; other panels depict staining with corresponding antibodies (scale bar 150 μm in all panels). (E–I) Quantification of IHC staining intensity of slides from panel D. Each dot represents one tumour (relative IHC intensity, mean of n=4–5 ± SD (one-tailed t-test). (J) Immunofluorescent staining of allografted tumours. The scale bar is 30 μm. (K) Flow-cytometric quantification of F4/80-MHCII double-positive (M1) TAMs from tumours in panel B. Each dot represents one tumour (mean±SD). (L) Flow-cytometric quantification of F4/80-CD206 double-positive (M2) TAMs from tumours in panel B. Each dot represents one tumour (mean±SD). (M) IHC of tumours from panel B. Arrows depict individual T cells. The scale bar is 100 μm. (N–S) Flow-cytometric quantification of T cell subtypes in WT/KO5.3 tumours. Each dot represents one tumour (mean±SD). DYRK1B, dual specificity and tyrosine phosphorylation-regulated kinase 1B; IHC, immunohistochemistry; KO, knockout; MHCII, major histocompatibility complex class II; PDAC, pancreatic ductal adenocarcinoma; TAM, tumour-associated macrophages; WT, wild-type.

(figure 3G,H). One of the most striking differences between WT and KO was however observed with F4/80, revealing a significantly increased abundance of macrophages in KO tumours (figure 3D,I), a finding also corroborated with the second KO clone (online supplemental figure S3C). Interestingly, TANs appeared not to be recruited (online supplemental figure S3D). Dual immunofluorescence, as well as flow cytometry studies, revealed that the KO-associated TAMs were TNF-positive and MHCII-positive, suggesting a polarisation towards an M1-like state (figure 3J,K and online supplemental figure S3E). In contrast, the M2-marker CD206 was unaffected by the *Dyrk1b* genotype (figure 3L and online supplemental figure S3F,G). The increased influx of macrophages (Mphs) into KO tumour tissue was also reflected in the corresponding RNAseq data set, where pan-Mph genes (*Cd68* and *Msr1*), as well as M1-polarised Mph genes (*Cd80* and *Csf2*) presented with significantly higher levels in KO tumours (online supplemental figure S3H,I). In contrast, M2-polarised Mph genes (*Cd163* and *Serpinb2*) trended to an inverse correlation (online supplemental figure S3J). Interestingly, and in contrast to the cancer cells, the majority of the KO-associated TAMs were non-proliferative (online supplemental figure S3K–M), strongly suggesting that they were recruited to the tumour site and not generated by proliferative expansion of a resident pool.

As TAMs can impact T-cell differentiation and activation, we next investigated WT/KO tissue for the presence of CD4^{+} and CD8^{+} T cells and found the former to be more frequent in KO versus WT tumours (figure 3M–O). Importantly, these CD4^{+} cells were highly enriched for the Th1 markers interferon-gamma (IFNγ), TNF and T-bet (figure 3P,Q and online supplemental figure S3N,O). Considering that Th1 cells can boost M1-TAM activation, these results point towards a reciprocal crosstalk between Th1 and M1-TAMs in the *Dyrk1b*-deficient TME. In contrast, the frequency of neutrophil-attracting RORγt^{+} Th17 cells was significantly reduced (figure 3R). We also observed an increased presence of IFNγ^{+}/TNF^{+} CD8^{+} T-cells, indicating enhanced differentiation of cytotoxic lymphocytes, despite comparable absolute frequencies in WT versus KO tumours (online supplemental figure S3S).

In conclusion, we find the loss of *Dyrk1b* to exert a strong growth inhibition in an in vivo setting, despite fostering cell proliferation in vitro. This tumour-suppressive effect was associated with a strong influx of Mphs, which in addition showed signs of a tumoricidal M1 polarisation. In line with the known crosstalk of M1-like TAMs with Th1 cells, we observed their increased abundance in KO tumour tissue.

A *Dyrk1b*-controlled cancer cell secretome acts on several aspects of Mph physiology

Next, we were eager to decipher the *Dyrk1b*-dependent cellular effects imparted by tumour cells on macrophages. Assuming secreted factors to be essential for this crosstalk, we generated conditioned SNs derived from WT or KO mKpc4 cells and applied them to primary mouse BMDM (figure 4A). First, we analysed the transcriptomic alterations in Mphs on exposure to SN of WT or KO cells. As evident from figure 4B, KO-SN induced many innate immune-related gene signatures (lipopolysaccharide, interferon, polyI:C-RNA, TNF) in Mphs as compared with WT-SN, largely resembling the situation observed in KO tumours (figure 3C). Downregulated genes surprisingly include not only several immune-associated pathways but also a range of proinflammatory signatures such as IL1B, leucocyte migration, inflammatory response, IL10 or IL13 (figure 4C). This unexpected

dichotomy was in fact also apparent when individual Mph activation markers were analysed in more detail (figure 4D). While SN from *Dyrk1b*-KO tumour cells induced several M1-associated genes (eg, *Ccl5* and *Cd40*), it downregulated the expression of inflammatory M1-like (eg, *Il1a* and *Il1b*) as well as M2-associated genes (eg, *Arg1* and *Serpinb2*) (figure 4D and online supplemental figure S4A–C). A similar pattern of expression changes was also observed in human primary peripheral blood-derived macrophages exposed to SN from human PDAC cells, in which *DYRK1B* was knocked down by shRNA (see online supplemental figure S4D–F for cell characterisation and online supplemental figure S4G–I for effects on Mphs). Furthermore, these results were recapitulated by treating primary murine Mphs with SN from mKpc4 cells previously exposed to the DYRK1B-inhibitor AZ191 (figure 4E–G). Thus, using several different systems, these data imply that loss of tumour cell DYRK1B reshapes the cancer secretome, yielding an M1-like Mph phenotype with reduced inflammatory potential.

In addition to the effects on Mph polarisation, KO-SN increased not only the overall viability (figure 4H) but also functioned as a potent chemoattractant for Mphs (figure 4I), providing a very likely explanation for why KO tumours contained such high numbers of TAMs (figure 3D,I). Beyond these observations in the mouse system, comparable findings were also made with human PDAC cells and human Mphs (online supplemental figure S4J).

In light of the fact that *Dyrk1b* KO tumours were significantly smaller than their WT counterparts and, in addition, contained high numbers of TAMs, we reasoned that the phagocytic activity of Mphs might contribute to this growth inhibition. To assess this issue, we labelled tumour cells and primary Mphs with separate fluorescent dyes and monitored the appearance of double-positive cells (indicative of tumour cell engulfment by Mphs) in co-culture (figure 4J). Intriguingly, loss of *Dyrk1b* in tumour cells significantly enhanced their phagocytosis by co-cultured Mphs (figure 4K and online supplemental figure S5A), a finding which was successfully recapitulated in human cells (online supplemental figure S4B,C). Moreover, small molecule-mediated DYRK1B inhibition also led to increased tumour cell phagocytosis in mouse (online supplemental figure S5D,E) and human (online supplemental figure S5F,G) cancer cells.

In order to elucidate whether the increased phagocytic effect required direct cell–cell contact between Mphs and target cells in co-culture or was caused by secreted factors, we pretreated Mphs with SN from WT or KO tumour cells prior to the measurement of phagocytosis of WT mKpc4 as target cells (figure 4L). Importantly, these experimental conditions abrogated the increased phagocytic ability imposed by KO cells observed in direct co-culture experiments before (figure 4K), indicating that direct tumour cell-Mph contact was necessary for the enhanced engulfment of KO tumour cells by Mph. A similar result was obtained with human PDAC cells (online supplemental figure S5H).

Motivated by our previous observation on reduced inflammatory CAF (iCAF) numbers in *Dyrk1b* KO tumours (figure 3D,H), we analysed a possible crosstalk between Mphs and CAFs. Specifically, we collected SN from WT or KO cancer cells and treated Mphs (figure 4M). Subsequently, PSCs were exposed to conditioned media from these Mphs and myCAF/iCAF polarisation was assessed by qRT-PCR. In line with our previous results obtained in vivo (figure 3D,H) as well as in vitro (figure 4D,F), *Dyrk1b*-KO-SN-treated Mphs failed to induce an iCAF phenotype, whereas the corresponding *Dyrk1b*-WT-treated Mphs successfully did (figure 4N,O). In summary, tumour cell DYRK1B was found to affect multiple aspects of Mph functionality, that is, polarisation, migration, viability
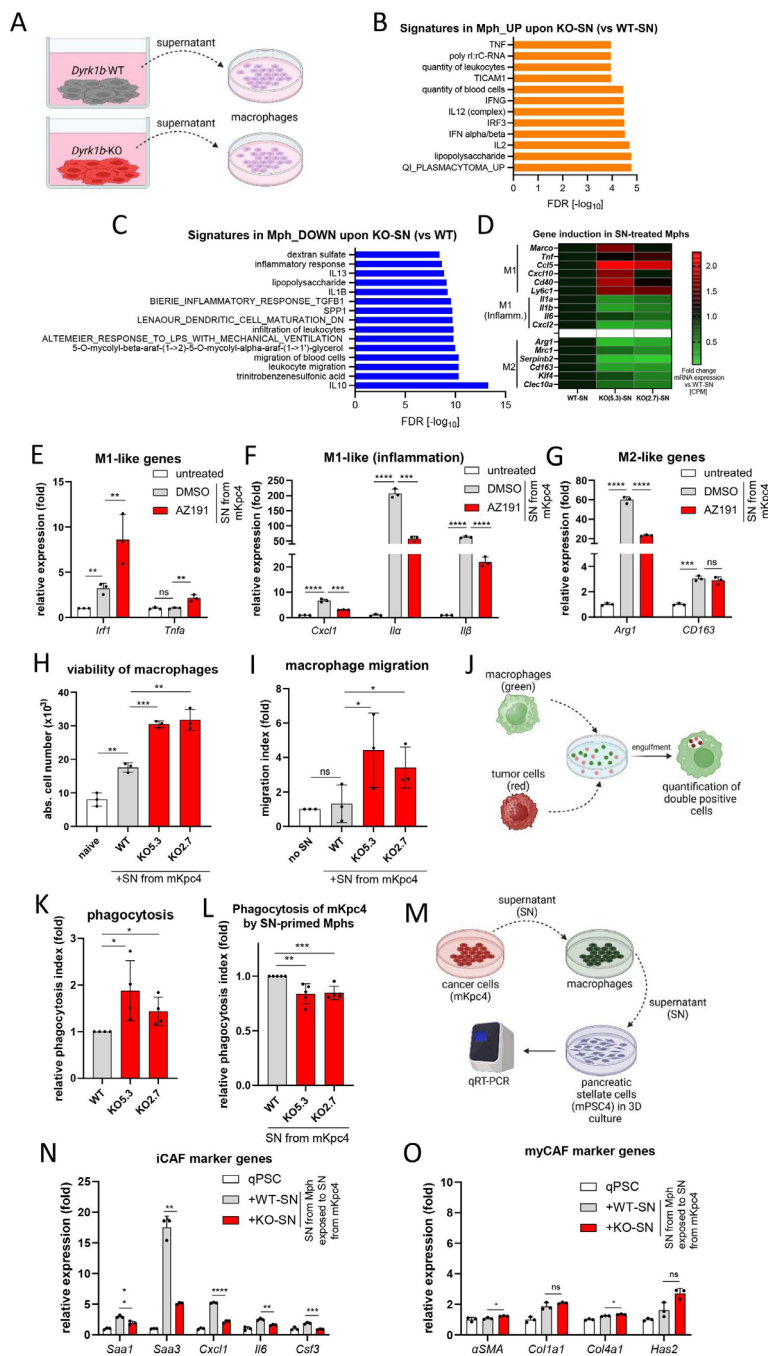
Figure 4 *Dyrk1b*-controlled cancer cell physiology acts on several aspects of Mph functions. (A) Scheme depicting the experiments to analyse the impact of the tumour cell secretome on Mphs. (B) Transcriptome signatures (RNAseq) of upregulated genes in Mphs after exposure to KO5.3 SN from mKpc4 cells. (C) Transcriptome signatures (RNAseq) of downregulated genes in Mphs after exposure to KO5.3 SN from mKpc4 cells. (D) Changes in expression of individual Mph genes (RNAseq) upon treatment with the indicated SN. (E–G) Relative mRNA expression determined by qRT-PCR of M1-like and M2-like genes in mouse BMDM (either untreated or stimulated with SN collected from WT mKPC4 cells previously treated with DMSO as a solvent or with 1 µM AZ191 for 4 days. Shown is one representative of n=3–7, measured in triplicate (mean±SD). (H) Absolute BMDM cell number left untreated (naive) or stimulated with conditioned media collected from WT/KO mKpc4 cells. Shown is one representative of n=3, measured in triplicate (mean±SD). (I) Migration over 16 hours of BMDM towards plain 0.5% containing medium (no SN) or medium containing 50% of SN from WT or KO mKpc4 cells. Mean of n=3±SD. (J) Graphical outline of the phagocytosis assay. BMDMs were labelled in green and tumour cells in red. Phagocytic Mphs were identified as double-positive cells. (K) The relative capability of BMDM to phagocytose WT or KO mKpc4 cells (calculated as a percentage of double-positive Mphs). Mean of n=4±SD. (L) The relative capability of BMDM to phagocytose WT mKpc4 cells. Before the phagocytosis assay, BMDM were primed with SN from WT or KO mKpc4 cells for 24 hours. Mean of n=5±SD. (M) Experimental scheme for crosstalk between cancer cells, Mphs and PSCs (mPSC4). (N–O) Relative mRNA expression determined by qRT-PCR of inflammatory (iCAF) and myofibroblastic (myCAF) cancer-associated fibroblast (CAF) marker genes in mPSC4 cells either left untreated (qPSC) or treated with SN from BMDM stimulated with SN from WT or KO5.3 mKpc4 cells. Shown is one representative of n=4, measured in triplicate (mean±SD). BMDM, bone-marrow-derived macrophages; DMSO, dimethyl sulfoxide; DYRK1B, dual specificity and tyrosine phosphorylation-regulated kinase 1B; KO, knockout; Mphs, macrophages; PSC, pancreatic stellate cells; qPSC, quiescent PSC; qRT-PCR, quantitative reverse transcription PCR; SN, supernatant; WT, wild-type.

and, possibly most importantly, phagocytic activity. All of the observed processes possess tumoricidal potential and might thus be harnessed therapeutically.

DYRK1B regulates the 'don't eat me' signal CD24 to prevent destruction by macrophages

In our attempts to understand the DYRK1B-mediated interactions between cancer cells and Mphs in greater detail, we determined differentially secreted factors by means of cytokine arrays. As depicted in figure 5A,B, several paracrine signalling molecules, such as CCL20, CX3CL1, PCSK9 or VEGF, were found to be downregulated by *Dyrk1b* loss (figure 5A,B). In contrast, levels of secreted CCL5, CCL6, CXCL2, CXCL10 or MCSF were increased in *Dyrk1b*-depleted cancer cell SN. Since many of the upregulated factors are known to possess chemo-attractant properties, we individually eliminated their activity by adding neutralising antibodies and measured their contribution to the overall migratory potential of Mph. These experiments demonstrated that several of the mediators identified significantly contributed to the *Dyrk1b*-dependent increased attraction of Mph to *Dyrk1b*-null cells (figure 5C). In addition, we performed mass-spectrometric secretome studies, which revealed, among others, inhibin βA (Inhba; a member of the TGFβ superfamily) as a ligand specifically upregulated in the KO secretome (figure 5D). Moreover, semaphorin 3e (Sema3e) was found to be downregulated in KO SN (figure 5D). Sema3e had previously been described as a proinflammatory protein in lipopolysaccharide-treated macrophages.[43] Indeed, when we exposed primary Mph to recombinant Sema3e protein, we observed an upregulation of M2-associated *Arg1* mRNA expression, while M1-associated *Tnf* was concomitantly downregulated (figure 5E). In summary, we identified several *Dyrk1b*-regulated paracrine signalling molecules involved in Mph attraction/migration and polarisation.

A range of membrane receptors on target cells with relevance to phagocytosis have been discovered in recent years, such as CD24, CD47 or B2M.[11 44 45] Among these phagocytosis checkpoint proteins, CD24 appeared of particular interest as we observed a downregulation of total CD24 protein in *Dyrk1b*-KO cell clones (figure 5F). Remarkably, not only total protein levels but also cell surface-localised CD24 were significantly reduced on *Dyrk1b* loss (figure 5G and online supplemental figure S5I). In contrast, *Cd24* mRNA levels were not uniformly reduced in both clones, arguing for a certain degree of post-transcriptional control of CD24 by DYRK1B (figure 5H). CD24 levels were also lower in tumours derived from *Dyrk1b*-KO versus WT cells (figure 5I,J). Furthermore, lower total and cell surface CD24 protein levels could also be observed upon pharmacological DYRK1B inhibition (online supplemental figure S5J–L), despite unaltered *Cd24* mRNA expression (online supplemental figure S5M). In addition, human PDAC cells with stable *DYRK1B* knockdown supported the findings above and also displayed reduced total (figure 5K) as well as cell-surface-localised CD24 protein levels (figure 5L and online supplemental figure S5N). In these *DYRK1B*-KD cells, *CD24* mRNA levels were reduced by approximately half (online supplemental figure S5O). In total, we provide experimental evidence that DYRK1B regulates Mph biology on several levels. The kinase not only modulates the paracrine secretome impinging on Mph recruitment and polarisation but also increases the cell-autonomous levels of 'immunologically self'-associated CD24, thereby protecting cancer cells from phagocytic innate immune attack.

A DYRK1B-directed therapy extends survival in an autochthonous mouse model of PDAC

In order to assess the therapeutic value of DYRK1B targeting, we made use of the well-established and highly aggressive KPC mouse model.[39] Pancreatic tumour development in KPC animals was allowed up to approximately $100-150\,mm^3$, from which time point on control animals typically survived for another 2 weeks. Pharmacological treatment was initiated at this stage and tumour sizes were regularly determined by ultrasound until the animals had to be sacrificed (figure 6A). The treatment regimen consisted of three components: (1) gemcitabine (Gem; 70 mg/kg; once a week) as one of the current standards of clinical care; (2) AZ191 (AZ; 5 mg/kg; two times per week) as a specific DYRK1B inhibitor and (3) KU0063794 (KU; 5 mg/kg; two times per week), a dual mTOR inhibitor synergising with DYRK1B inhibition in vitro (figure 2F,G). Importantly, this triple therapy was very well tolerated by the animals and no obvious toxicity or gross changes in body weight were observed during treatment (figure 6B). This was in particular contrast to gemcitabine treatment, which resulted in a significant treatment-related drop in body weight, indicative of chemotherapy-induced toxicity. Surprisingly, this decline in body weight was absent in triple-treated animals, despite the fact that this medication included gemcitabine as well (figure 6C).

Moreover, and in agreement with the disappointing impact of chemotherapy in the clinic, single treatment with gemcitabine led to no detectable improvement in the survival of KPC animals (online supplemental figure S6A). Furthermore, monotherapy with AZ191 did not significantly impact life span (online supplemental figure S6B), but an increased TAM abundance could be observed in AZ-treated tissues (online supplemental figure S6C,D). To our surprise, combined DYRK1B/mTOR inhibition (AZ/KU) also did not extend survival (online supplemental figure S6E), but combining AZ191 with gemcitabine yielded a modest but significant extension of survival in the treated animals (online supplemental figure S6F). The greatest effects were, however, achieved by employing the AZ/KU/Gem triple therapy, resulting in pronounced tumour stasis over an extended period of time (figure 6D). The overall survival of treated mice was significantly prolonged, from a median of 15 days in vehicle-treated control animals to 23 days in the triple-treated cohort (figure 6E). Analysing treatment time-matched solvent and triple-therapy tumour samples (2 weeks of treatment) confirmed significant CD24 downregulation (figure 6F) as well as increased Mph recruitment into tumour tissue in the latter cohort (figure 6G,H). Strikingly, the triple therapy cohort consisted of two clearly distinct subgroups of almost equal size: while one group did not respond at all to treatment and displayed a median survival (14 days) comparable to the control group, the responder subgroup had a significantly prolonged overall median survival of 33 days, thus extending the life span of tumour-bearing KPC mice by more than twofold (figure 6I). At the endpoint, increased macrophage abundance was selectively associated with the responder group, whereas the non-responder animals displayed F4/80-positivity comparable to the solvent cohort (figure 6J,K). These data suggest that a successful therapy response was linked to effective and/or sustained Mph recruitment into the tumour tissue. In summary, we thus present in vivo evidence for a well-tolerated drug combination resulting in strong macrophage recruitment and a significant extension of survival in a highly aggressive autochthonous PDAC mouse model.
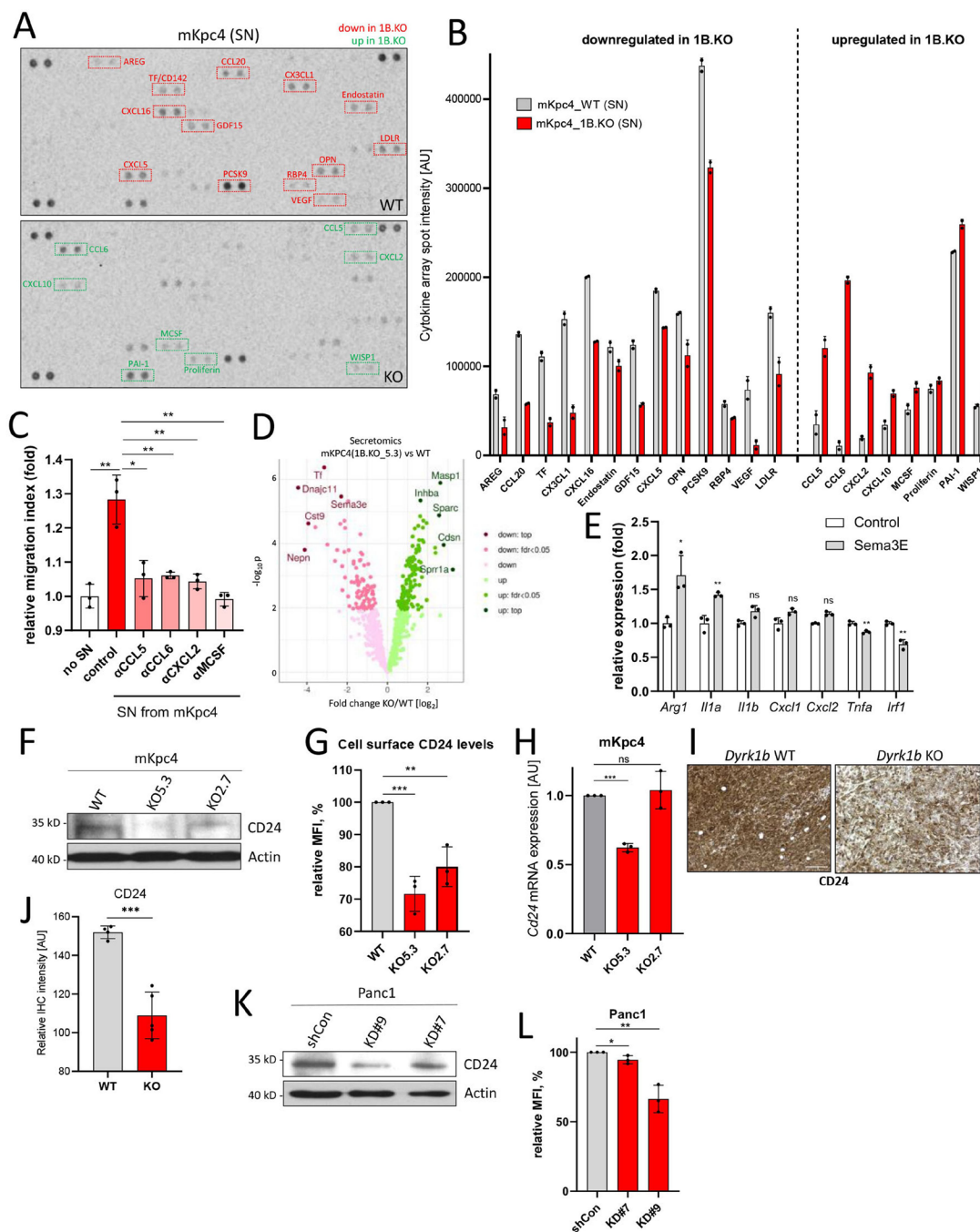
Figure 5 DYRK1B-dependent cancer cell impact on macrophage physiology. (A) Mouse cytokine array membranes incubated with SN from WT/KO mKpc4 cells. Cytokines and chemokines downregulated or upregulated in *Dyrk1b*-KO clone 5.3 (vs WT) are highlighted in red and green, respectively. (B) Quantification of the results depicted in A (duplicate spots). (C) Migration index of BMDM towards SN collected from WT mKpc4 cells plus either no antibody (control) or supplemented with neutralising antibodies against the indicated chemokines. Shown is the mean of one representative of n=3, measured in triplicate wells (±SD). (D) The volcano plot of proteins differentially secreted by WT or KO5.3 mKpc4 cells was detected by mass spectrometry-based proteomics. Proteins upregulated or downregulated in *Dyrk1b*-KO are highlighted in green and red, respectively. Modelled effect sizes and nominal p values are plotted, while luminosity maps to false discovery rate-corrected p values <0.05 (n=3). (E) Relative mRNA expression was determined by qRT-PCR of M1-like and M2-like marker genes in untreated BMDM (control) or in BMDM treated with 100 ng/mL recombinant Sema3E. Shown is one representative of n=2, measured in triplicate (mean±SD). (F) Western blot depicting endogenous CD24 protein levels in WT/KO mKpc4 cells. Actin was used as a loading control. Shown is one representative blot of n=2. (G) Relative MFI of surface CD24 on WT/KO mKpc4 cells. Mean of n=3±SD. (H) The relative *Cd24* mRNA expression as determined by qRT-PCR in WT/KO mKpc4 cells. Mean n=3±SD. (I) CD24 IHC of *Dyrk1b* WT/KO5.3 allograft tumour tissue. The scale bar is 100 µm. (J) Quantification of results from panel I. Each dot represents one tumour (mean±SD). (K) Western blot depicting CD24 protein level in parental Panc1 cells (WT) and *DYRK1B*-knockdown clones #9 and #7. Actin was used as a loading control. Shown is one representative blot of n=2. (L) Relative MFI of surface CD24 on parental Panc1 cells (WT) and *DYRK1B*-knockdown clones #7 and #9. Mean of n=3±SD. BMDM, bone-marrow-derived macrophages; DMSO, dimethyl sulfoxide; DYRK1B, dual specificity and tyrosine phosphorylation-regulated kinase 1B; KO, knockout; MFI, mean fluorescence intensity; Mphs, macrophages; PSC, pancreatic stellate cells; qPSC, quiescent PSC; qRT-PCR, quantitative reverse transcription PCR; SN, supernatant; WT, wild-type.
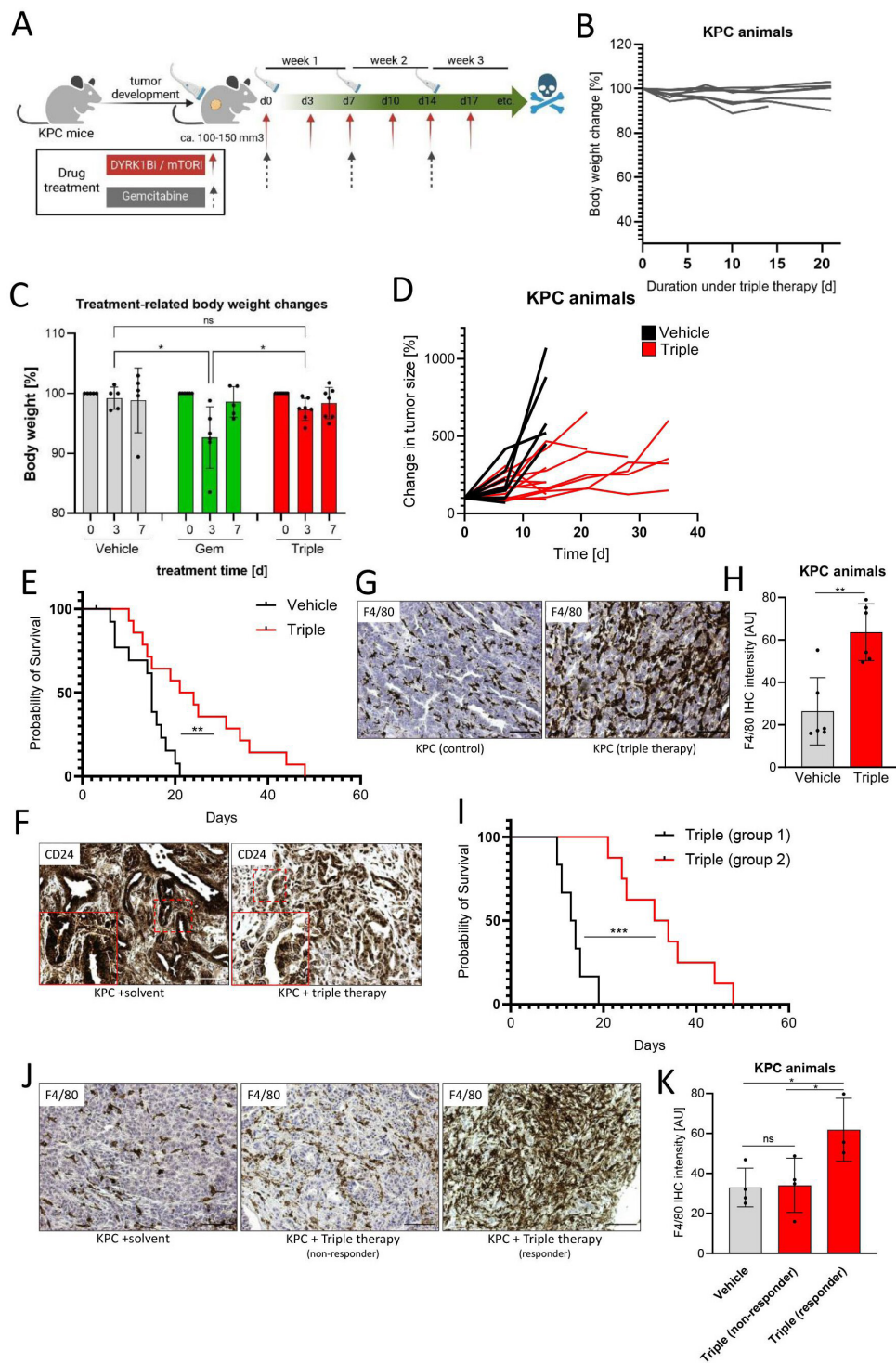
Figure 6 A DYRK1B-directed therapy extends survival in an autochthonous mouse model of PDAC. (A) Schematic outline of the treatment of KPC mice with drugs. Triple-mutant (LSL-Kras$^{G12D/+}$, LSL-Trp53$^{R172H/+}$ and Pdx1-Cre) animals underwent weekly palpation to identify tumour initiation. When a tumour reached 100–150 mm^3, mice were treated with gemcitabine (Gem; 70 mg/kg; once a week), AZ191 (DYRK1Bi; 5 mg/kg; two times per week) and KU0063794 (mTORi; 5 mg/kg; two times per week) according to the scheme. (B) Body weight change of KPC mice undergoing triple therapy (Gem/AZ/KU). Each line represents one animal. (C) Early changes in body weight in the control (vehicle), Gem and triple regimen arms. The first treatment was given on day 0. Each dot represents one animal (mean±SD). (D) Change in tumour size of KPC mice treated with vehicle (solvent; black lines) or triple therapy (red lines). Each line represents one animal. (E) Kaplan-Meier overall survival curve of KPC mice treated with vehicle (black line, n=13) or with triple therapy (red line, n=14) (log-rank test). (F) CD24 IHC of tumours after a 14-day solvent/triple therapy. The scale bar is 100 μm. (G) Representative F4/80 IHC staining of KPC tumours receiving 14 days of the vehicle or triple treatment. The scale bar is 100 μm. (H) Quantification of F4/80 staining intensity as shown in G. Each dot represents one tumour (mean of n=6±SD). (I) Kaplan-Meier overall survival curve of KPC mice treated with triple therapy. Black line: non-responders (n=6); red line: responders (n=8) (log-rank test). (J) F4/80 IHC at endpoint in control animals and in triple therapy responders/non-responders. The scale bar is 100 μm. (K) Quantification of F4/80 IHC as depicted in panel J (mean±SD; one-tailed t-test). DYRK1B, dual specificity and tyrosine phosphorylation-regulated kinase 1B; IHC, immunohistochemistry; PDAC, pancreatic ductal adenocarcinoma.

Intratumoural macrophage abundance correlates with DYRK1B levels in human patients with PDAC

Next, we aimed to validate our findings in human patients. To this end, we first made use of the Marburg cohort of patients with PDAC, whose tissue was stained by immunohistochemistry for the pan-macrophage marker CD68 (n=46). In parallel, we quantified *DYRK1B* expression levels by bulk mRNA sequencing of the same patient samples. As *DYRK1B* is mostly expressed by tumour cells (figure 1D), bulk expression was used as a proxy for epithelial *DYRK1B* levels. Intriguingly, patient samples with high *DYRK1B* expression displayed low Mph infiltration, while the reverse was true for patients with low *DYRK1B* levels (figure 7A). In order to extend and verify this negative correlation, we performed a tertiary split of the samples based on their *DYRK1B* expression and determined the macrophage abundance in these tissues by quantifying the immunohistological CD68 staining intensity. As presented in figure 7B, *DYRK1B* levels are significantly associated in a negative manner with Mph presence in human PDAC tissue samples (figure 7B). Moreover, *CD24* transcript levels were specifically increased in the *DYRK1B*-high subgroup within this patient cohort (figure 7C).

Furthermore, we extended our investigation to an independent human PDAC dataset (TCGA cohort; n=178) and again observed significant negative correlations between *DYRK1B* expression and the pan-Mph marker genes *CD68* (figure 7D), *MSR1* (figure 7E), *ITGAM* (encoding for CD11B; figure 7F) or the M1-associated genes *CD86* (online supplemental figure S7A) and *MHCII* (*HLA-DRA*; online supplemental figure S7B). A third human PDAC dataset (Yang cohort; n=139)[46] further supported the anticorrelation of *DYRK1B* expression to Mph genes *MSR1* (online supplemental figure S7C), *CD80* (online supplemental figure S7D) and *CD86* (online supplemental figure S7E). In conclusion, the negative correlation between *DYRK1B* and Mph infiltration is not only observed in murine systems but also validated in human PDAC patient material.

DISCUSSION

Novel and clinically actionable drug targets are of high interest in translational pancreatic cancer research. Here, we describe the DYRK1B kinase as such a drug target, a protein belonging to the underexplored but potentially promising 'dark kinome'. Small-molecule inhibitors of DYRK1 kinases are currently in clinical phase I testing and, if successful, will soon be available for clinical PDAC translation. Targeting the c-MET-modulating paralogue DYRK1A has previously proven promising in preclinical PDAC models[22] and, hence, inhibitors that would block both class I DYRK family members appear worth evaluating. With respect to DYRK1B, its role in cancer cells appears paradoxical at first: the kinase suppresses cell cycle-promoting factors such as cyclin D1,[20] stabilises cell cycle-inhibiting proteins like p27[40] and promotes the assembly of the antiproliferative transcriptional DREAM complex.[41] Despite these seemingly tumour-suppressive effects, DYRK1B is found overexpressed in many cancers, including PDAC, where it mediates cellular quiescence, motility and cell survival.[47] In pancreatic cancer, point mutations in *DYRK1B* are rare, but its mRNA is frequently upregulated[17] or its gene is chromosomally amplified.[36] In addition, common molecular hallmarks of PDAC, such as mutant KRAS or hypoxia, activate DYRK1B's kinase activity.[48 49] Given this apparent contradictory evidence, it thus remained elusive how DYRK1B functions as a pancreatic cancer oncogene. We here provide evidence that DYRK1B has a pronounced impact on the secretome of cancer cells, in turn modulating the cellular makeup of the TME. Most importantly, this TME effect is dominant over the cell-intrinsic cell cycle control.

Specifically, we could show that DYRK1B regulates the abundance of macrophages (Mphs) in tumours. Our data further demonstrate DYRK1B's kinase activity to be required for this effect and that, as a result, DYRK1B inhibitors are an attractive option to restructure the myeloid TME. The DYRK1B-inhibited TME consists of M1-like-polarised TAMs together with increased numbers of activated IFNγ/TNF-producing T-bet⁺ Th1 cells, generating an effective tumour-suppressive environment. In this context, it is interesting to note that macrophage-intrinsic DYRK1B has also been implicated in M1/M2 polarisation,[50] and DYRK1B inhibition may synergise with TAM control through cancer cell-intrinsic DYRK1B. Intriguingly, DYRK1B also suppresses the direct recognition of cancer cells by Mphs through upregulation of the 'don't eat me' signal CD24 on tumour cells, a process that presumably is post-transcriptional.

DYRK1B thus appears to modulate Mph-mediated immunity by several means: through soluble factors, it affects Mph migration, viability and polarisation, while cell-intrinsic mechanisms affect target cell recognition and phagocytosis. Targeting other myeloid checkpoint molecules in PDAC has been suggested before CD47-blocking antibodies slowed disease progression and prolonged survival in a mouse model,[51] reduced cancer stem cell pools,[52] but have encountered challenges such as anaemia and thrombocytopenia. β2-microglobulin shields cancer cells from different malignancies from phagocytic attack[45] but was not expressed in our cells.

As one of the factors driven by DYRK1B, we remarkably identified the axon guidance molecule Semaphorin 3E (Sema3e), which has been associated with poor prognosis in PDAC and was found to impinge on Mph-based inflammation,[43 53] thus making it an interesting anticancer target regulated by DYRK1B. Targeting DYRK1B in tumour cells also upregulated the chemokines MCSF, CCL5, CCL6 and CXCL2, all of which are known to recruit macrophages to the tumour site. A majority of studies so far suggest that blocking MCSF/CCL6/CCL5/CXCL2 pathways could unleash the antitumorigenic potential of macrophages.[54 55] However, a high infiltration of the tumour site with tumoricidal macrophages might effectively kill tumour cells and may potentially be combined with phagocytosis checkpoint therapies. DYRK1B inhibitors may, in this respect, serve as a multifaceted tool to attract tumoricidal macrophages and facilitate the phagocytosis of cancer cells.

In our attempts to define drug combinations with promising translational potential, we combined a DYRK1B inhibitor with a synergising mTOR blocker. While this combination proved powerful in cell culture, we were surprised to see it fail in vivo. In addition, we included the commonly used chemotherapeutic agent gemcitabine in the combination, as it is considered to target cells leaving quiescence upon DYRK1B inhibition.[21] This triple combination was surprisingly well tolerated by the treated animals, with no signs of toxicity and no overt loss in body weight and yielded a life span extension of more than twofold in many tumour-bearing KPC animals, which, to our knowledge, not many preclinical pharmacological regiments are able to achieve. It is, however, noteworthy that only approximately half of the animals responded to the medication. Therapy response hereby appeared to necessitate Mph recruitment as non-responders lacked signs of increased Mph infiltration. The exact mechanisms underlying this dichotomous therapy response as well as biomarkers predicting it require future work, as does the question of why the tumoricidal impact is transient and animals eventually succumb to the disease despite treatment continuity.
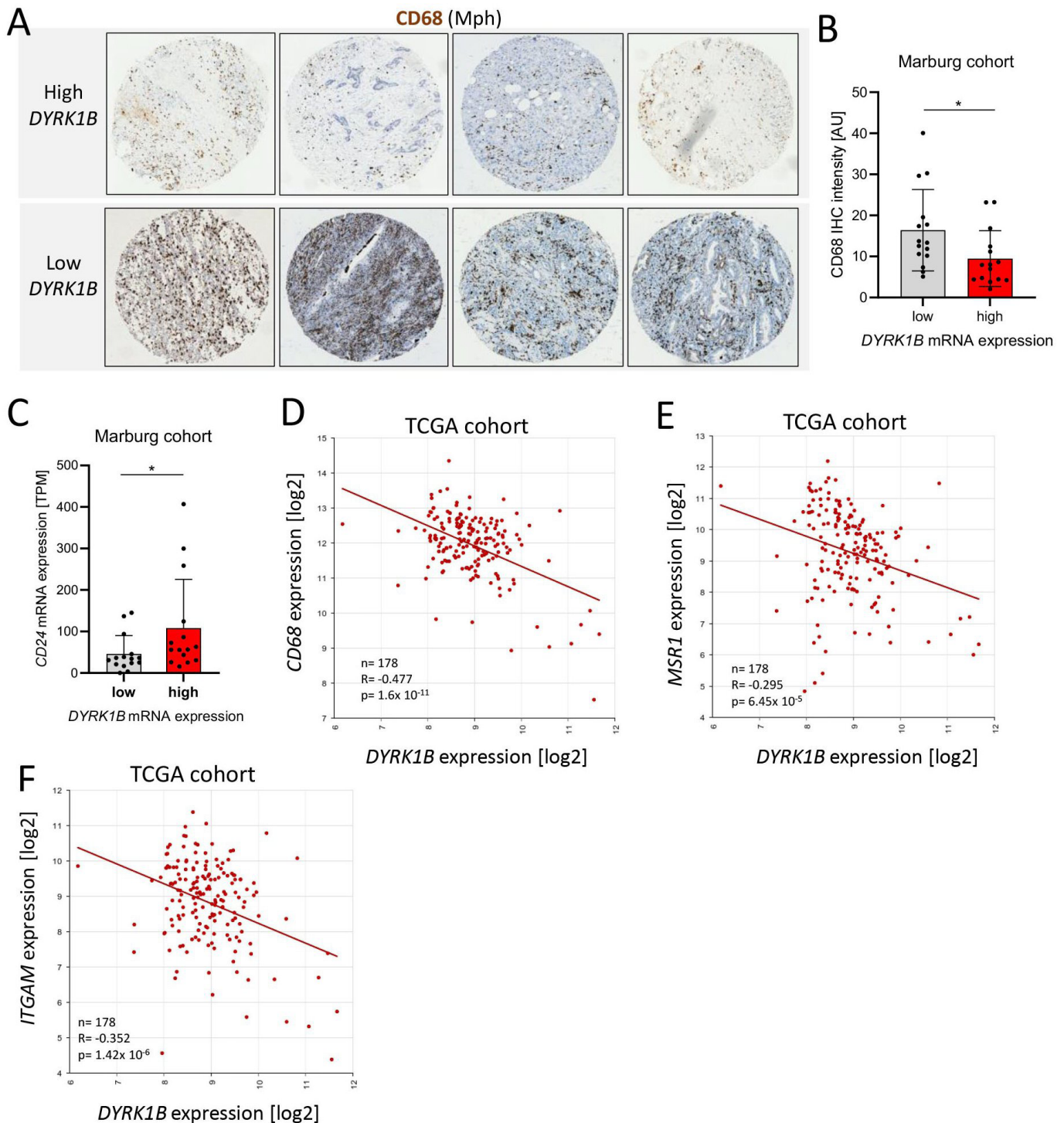
Figure 7 Intratumoral macrophage abundance correlates with DYRK1B levels in human PDAC. (A) Immunohistochemical CD68 staining (brown) of human PDAC tissue microarrays (Marburg cohort). *DYRK1B* levels were determined by bulk RNAseq. (B) Quantification of CD68 immunohistochemistry intensity in patients with PDAC, which were split into *DYRK1B*-low and high subgroups (n=15 each). Each dot represents one patient tumour (mean±SD). (C) *CD24* mRNA levels in patients with PDAC as assessed by bulk RNA sequencing. Patients were split into *DYRK1B*-low/high subgroups (n=15 each). Each dot represents one patient tumour (mean±SD). (D) Correlation between *CD68* and *DYRK1B* bulk mRNA expression in patients with PDAC of the TCGA cohort. (E) Correlation between *MSR1* and *DYRK1B* bulk mRNA expression in patients with PDAC of the TCGA cohort. (F) Correlation between *ITGAM* (encoding CD11B) and *DYRK1B* bulk mRNA expression in patients with PDAC of the TCGA cohort. DYRK1B, dual specificity and tyrosine phosphorylation-regulated kinase 1B; PDAC, pancreatic ductal adenocarcinoma; mRNA, messenger RNA; TCGA, The Cancer Genome Atlas.

Our findings significantly extend insight into DYRK1B biology and show this kinase does not act as a mere negative cell cycle regulator. In fact, one might speculate that DYRK1B's wider oncogenic role lies in executing tumour cell protecting measures to create a 'safe haven'. This may include the induction of proliferative quiescence, cell survival and DNA repair to

evade chemotherapy on the one hand, but also the promotion of immune evasion to circumvent attacks from the host immune system on the other. Concerning the latter, DYRK1B may represent a particularly valuable target as it acts on multiple layers to control macrophage immunity, affecting not only recruitment, viability and polarisation but also upregulating the innate immune checkpoint CD24. It will thus be interesting to explore whether DYRK1B-directed therapy may be potentiated by the addition of either immune checkpoint blockade (αPD-1/PD-L1; α-CTLA4) or myeloid-stimulating approaches such as α-CD40 ligands. With the advent of clinical DYRK1 inhibitors, our data provide the groundwork for further combinatorial studies targeting this kinase for improved PDAC therapy.

Author affiliations
[1]Department of Gastroenterology Endocrinology and Metabolism, Center for Tumor and Immune Biology, Marburg, Germany
[2]Present address: Institute of Systems Immunology, Center for Tumor and Immune Biology, Marburg, Germany
[3]Institute of Systems Immunology, Philipps-Universitat Marburg, Marburg, Hessen, Germany
[4]Genomics Core Facility, Philipps University Marburg, Marburg, Germany
[5]Institute for Molecular Oncology, German Center for Lung Research (DZL), Marburg, Germany
[6]Max Planck Institute for Heart and Lung Research, Bad Nauheim, Germany
[7]Institute of Translational Proteomics, Philipps University, Marburg, Germany
[8]Medicinal Chemistry Core Facility, Philipps University Marburg, Marburg, Germany
[9]Department of Medicinal chemistry, Center for Tumor and Immune Biology, Marburg, Germany
[10]Bioinformatics Core Facility, Center for Tumor and Immune Biology, Marburg, Germany
[11]Institute for Medical Bioinformatics and Biostatistics, Institute for Molecular Biology and Tumor Research, Marburg, Germany
[12]Department of Visceral, Thoracic and Vascular Surgery, Philipps-University Marburg, Marburg, Germany
[13]Cell Imaging Core Facility, Center for Tumor Biology and Immunology, Philipps-University Marburg, Marburg, Hessen, Germany
[14]Institute of Pathology, University Hospital of Giessen-Marburg, Marburg, Germany
[15]Department of Gastroenterology, Endocrinology and Metabolism, Center for Tumor and Immune Biology, Marburg, Germany

Patient and public involvement Patients and/or the public were not involved in the design, or conduct, or reporting, or dissemination plans of this research.

Patient consent for publication Not applicable.

Ethics approval This study involves human participants and was approved by Ethics Committee University of Marburg (AZ 76-17). Participants gave informed consent to participate in the study before taking part.

Provenance and peer review Not commissioned; externally peer reviewed.

Data availability statement Data are available in a public, open access repository. Data availability: materials/methods data statement included. Datasets have been indicated in the clean manuscript version.

ORCID iDs
Anna Brichkina http://orcid.org/0000-0001-8707-9900
Matthias Lauth http://orcid.org/0000-0001-5922-5384

REFERENCES

1 Siegel RL, Miller KD, Wagle NS, *et al*. Cancer statistics, 2023. *CA Cancer J Clin* 2023;73:17–48.
2 Beatty GL, Werba G, Lyssiotis CA, *et al*. The biological underpinnings of therapeutic resistance in Pancreatic cancer. *Genes Dev* 2021;35:940–62.
3 Rahib L, Smith BD, Aizenberg R, *et al*. Projecting cancer incidence and deaths to 2030: the unexpected burden of thyroid, liver, and Pancreas cancers in the United States. *Cancer Res* 2014;74:2913–21.
4 Bärthel S, Falcomatà C, Rad R, *et al*. Single-cell profiling to explore Pancreatic cancer heterogeneity, plasticity and response to therapy. *Nat Cancer* 2023;4:454–67.
5 Bear AS, Vonderheide RH, O'Hara MH. Challenges and opportunities for Pancreatic cancer Immunotherapy. *Cancer Cell* 2020;38:788–802.
6 Huber M, Brehm CU, Gress TM, *et al*. The immune Microenvironment in Pancreatic cancer. *Int J Mol Sci* 2020;21:7307.
7 Zhu Y, Herndon JM, Sojka DK, *et al*. Tissue-resident Macrophages in Pancreatic Ductal adenocarcinoma originate from embryonic Hematopoiesis and promote tumor progression. *Immunity* 2017;47:323–38.
8 Stromnes IM, Burrack AL, Hulbert A, *et al*. Differential effects of Depleting versus programming tumor-associated Macrophages on engineered T cells in Pancreatic Ductal adenocarcinoma. *Cancer Immunol Res* 2019;7:977–89.
9 Helm O, Held-Feindt J, Grage-Griebenow E, *et al*. Tumor-associated Macrophages exhibit Pro- and anti-inflammatory properties by which they impact on Pancreatic tumorigenesis. *Int J Cancer* 2014;135:843–61.
10 Beatty GL, Chiorean EG, Fishman MP, *et al*. Cd40 agonists alter tumor Stroma and show efficacy against Pancreatic carcinoma in mice and humans. *Science* 2011;331:1612–6.
11 Barkal AA, Brewer RE, Markovic M, *et al*. Cd24 signalling through macrophage Siglec-10 is a target for cancer Immunotherapy. *Nature* 2019;572:392–6.
12 Feng M, Jiang W, Kim BYS, *et al*. Phagocytosis checkpoints as new targets for cancer Immunotherapy. *Nat Rev Cancer* 2019;19:568–86.
13 Singh R, Lauth M. Emerging roles of DYRK Kinases in Embryogenesis and hedgehog pathway control. *J Dev Biol* 2017;5:13.
14 Soppa U, Becker W. DYRK protein Kinases. *Curr Biol* 2015;25:R488–9.
15 Lindberg MF, Meijer L. Dual-specificity, tyrosine Phosphorylation-regulated Kinases (Dyrks) and Cdc2-like Kinases (Clks) in human disease, an overview. *Int J Mol Sci* 2021;22:6047.
16 Singh R, Dhanyamraju PK, Lauth M. Dyrk1B blocks Canonical and promotes non-Canonical hedgehog signaling through activation of the mTOR/AKT pathway. *Oncotarget* 2017;8:833–45.
17 Deng X, Ewton DZ, Li S, *et al*. The kinase Mirk/Dyrk1B mediates cell survival in Pancreatic Ductal adenocarcinoma. *Cancer Res* 2006;66:4149–58.
18 Deng X, Friedman E. Mirk kinase inhibition blocks the in vivo growth of Pancreatic cancer cells. *Genes Cancer* 2014;5:337–47.
19 Jin K, Ewton DZ, Park S, *et al*. Mirk regulates the exit of colon cancer cells from quiescence. *J Biol Chem* 2009;284:22916–25.
20 Zou Y, Ewton DZ, Deng X, *et al*. Mirk/Dyrk1B kinase Destabilizes Cyclin D1 by Phosphorylation at Threonine 288. *J Biol Chem* 2004;279:27790–8.
21 Ewton DZ, Hu J, Vilenchik M, *et al*. Inactivation of Mirk/Dyrk1B kinase targets quiescent Pancreatic cancer cells. *Mol Cancer Ther* 2011;10:2104–14.
22 Luna J, Boni J, Cuatrecasas M, *et al*. Dyrk1A modulates C-MET in Pancreatic Ductal adenocarcinoma to drive tumour growth. *Gut* 2019;68:1465–76.
23 Deng X, Hu J, Ewton DZ, *et al*. Mirk/Dyrk1B kinase is upregulated following inhibition of mTOR. *Carcinogenesis* 2014;35:1968–76.
24 Hupfer A, Brichkina A, Koeniger A, *et al*. Matrix stiffness drives Stromal Autophagy and promotes formation of a Protumorigenic niche. *Proc Natl Acad Sci U S A* 2021;118:e2105367118.
25 Jesnowski R, Fürst D, Ringel J, *et al*. Immortalization of Pancreatic Stellate cells as an in vitro model of Pancreatic fibrosis: Deactivation is induced by Matrigel and N-Acetylcysteine. *Lab Invest* 2005;85:1276–91.
26 Hwang RF, Moore T, Arumugam T, *et al*. Cancer-associated Stromal fibroblasts promote Pancreatic tumor progression. *Cancer Res* 2008;68:918–26.

27 Kettle JG, Ballard P, Bardelle C, *et al*. Discovery and optimization of a novel series of Dyrk1B kinase inhibitors to explore a MEK resistance hypothesis. *J Med Chem* 2015;58:2834–44.

28 Cunningham F, Allen JE, Allen J, *et al*. Ensembl 2022. *Nucleic Acids Res* 2022;50:D988–95.

29 Love MI, Huber W, Anders S. Moderated estimation of fold change and dispersion for RNA-Seq data with Deseq2. *Genome Biol* 2014;15:550.

30 Schneider P, Bayo-Fina JM, Singh R, *et al*. Identification of a novel actin-dependent signal Transducing Module allows for the targeted degradation of Gli1. *Nat Commun* 2015;6:8023.

31 Chevallet M, Diemer H, Van Dorsseaer A, *et al*. Toward a better analysis of secreted proteins: the example of the myeloid cells Secretome. *Proteomics* 2007;7:1757–70.

32 Cox J, Neuhauser N, Michalski A, *et al*. Andromeda: a peptide search engine integrated into the Maxquant environment. *J Proteome Res* 2011;10:1794–805.

33 Wu C-C, Jeratsch S, Graumann J, *et al*. Modulation of mammalian cardiomyocyte Cytokinesis by the extracellular matrix. *Circ Res* 2020;127:896–907.

34 Cox J, Mann M. Maxquant enables high peptide identification rates, individualized P. P.B.-Range mass Accuracies and Proteome-wide protein Quantification. *Nat Biotechnol* 2008;26:1367–72.

35 Kiweler M, Looso M, Graumann J. Marmoset - extracting publication-ready mass Spectrometry Metadata from RAW files. *Mol Cell Proteomics* 2019;18:1700–2.

36 Heidenblad M, Schoenmakers EFPM, Jonson T, *et al*. Genome-wide array-based comparative Genomic hybridization reveals multiple amplification targets and novel homozygous deletions in Pancreatic carcinoma cell lines. *Cancer Res* 2004;64:3052–9.

37 Stratford JK, Bentrem DJ, Anderson JM, *et al*. A six-gene signature predicts survival of patients with localized Pancreatic Ductal adenocarcinoma. *PLoS Med* 2010;7:e1000307.

38 Peng J, Sun B-F, Chen C-Y, *et al*. Single-cell RNA-Seq highlights intra-Tumoral heterogeneity and malignant progression in Pancreatic Ductal adenocarcinoma. *Cell Res* 2019;29:725–38.

39 Hingorani SR, Wang L, Multani AS, *et al*. Trp53R172H and Krasg12D cooperate to promote Chromosomal instability and widely metastatic Pancreatic Ductal adenocarcinoma in mice. *Cancer Cell* 2005;7:469–83.

40 Deng X, Mercer SE, Shah S, *et al*. The Cyclin-dependent kinase inhibitor P27Kip1 is stabilized in G(0) by Mirk/Dyrk1B kinase. *J Biol Chem* 2004;279:22498–504.

41 Litovchick L, Florens LA, Swanson SK, *et al*. Dyrk1A protein kinase promotes quiescence and Senescence through DREAM complex assembly. *Genes Dev* 2011;25:801–13.

42 Ashford AL, Oxley D, Kettle J, *et al*. A novel Dyrk1B inhibitor Az191 demonstrates that Dyrk1B acts independently of Gsk3Beta to Phosphorylate Cyclin D1 at Thr(286), not Thr(288). *Biochem J* 2014;457:43–56.

43 Mohammed A, Okwor I, Shan L, *et al*. Semaphorin 3E regulates the response of Macrophages to Lipopolysaccharide-induced systemic inflammation. *J Immunol* 2020;204:128–36.

44 Logtenberg MEW, Scheeren FA, Schumacher TN. The Cd47-SIRPα immune Checkpoint. *Immunity* 2020;52:742–52.

45 Barkal AA, Weiskopf K, Kao KS, *et al*. Engagement of MHC class I by the inhibitory receptor Lilrb1 suppresses Macrophages and is a target of cancer Immunotherapy. *Nat Immunol* 2018;19:76–84.

46 Yang S, Tang W, Azizian A, *et al*. Dysregulation of Hnf1B/Clusterin axis enhances disease progression in a highly aggressive subset of Pancreatic cancer patients. *Carcinogenesis* 2022;43:1198–210.

47 Boni J, Rubio-Perez C, López-Bigas N, *et al*. The DYRK family of Kinases in cancer: molecular functions and therapeutic opportunities. *Cancers (Basel)* 2020;12:2106.

48 Lee SB, Ko A, Oh YT, *et al*. Proline hydroxylation primes protein Kinases for Autophosphorylation and activation. *Mol Cell* 2020;79:376–89.

49 Jin K, Park S, Ewton DZ, *et al*. The survival kinase Mirk/Dyrk1B is a downstream Effector of Oncogenic K-Ras in Pancreatic cancer. *Cancer Res* 2007;67:7247–55.

50 Blom K, Rubin J, Berglund M, *et al*. Mebendazole-induced M1 Polarisation of THP-1 Macrophages may involve Dyrk1B inhibition. *BMC Res Notes* 2019;12:234.

51 Michaels AD, Newhook TE, Adair SJ, *et al*. Cd47 blockade as an adjuvant Immunotherapy for Resectable Pancreatic cancer. *Clin Cancer Res* 2018;24:1415–25.

52 Cioffi M, Trabulo S, Hidalgo M, *et al*. Inhibition of Cd47 effectively targets Pancreatic cancer stem cells via dual mechanisms. *Clin Cancer Res* 2015;21:2325–37.

53 Yong L-K, Lai S, Liang Z, *et al*. Overexpression of Semaphorin-3E enhances Pancreatic cancer cell growth and Associates with poor patient survival. *Oncotarget* 2016;7:87431–48.

54 Candido JB, Morton JP, Bailey P, *et al*. Csf1R+ Macrophages sustain Pancreatic tumor growth through T cell suppression and maintenance of key gene programs that define the squamous subtype. *Cell Rep* 2018;23:1448–60.

55 Steele CW, Karim SA, Leach JDG, *et al*. Cxcr2 inhibition profoundly suppresses metastases and augments Immunotherapy in Pancreatic Ductal adenocarcinoma. *Cancer Cell* 2016;29:832–45.

56 Rashid NU, Peng XL, Jin C, *et al*. Purity independent Subtyping of tumors (Purist), A clinically robust, single-sample Classifier for tumor Subtyping in Pancreatic cancer. *Clin Cancer Res* 2020;26:82–92.

Supplemental figure legends

Figure S1: The DYRK1B kinase is enriched in PDAC tumor cells.

A Genomic data on *DYRK1B* from the TCGA data set (www.cbioportal.org). **B** Kaplan-Meier plot depicting *DYRK1B*-associated overall survival of PDAC patients (n=146 patients, TCGA cohort, scan split, logrank test). **C** Single cell RNA sequencing results demarcating *DYRK1B*-expressing cells in human PDAC [1]. **D** Cell type-resolved *DYRK1B* mRNA expression (summarized reads) in human PDAC. Tumor cells are represented as "Ductal cell type 2"; normal ductal cells are named "Ductal cell type 1" [1]. **E** DYRK1B IHC of allografted WT/KO5.3 tumor tissue demonstrating antibody specificity. Mouse skeletal muscle was included as positive control for strong DYRK1B expression. Scale bar: 100 μm.

Figure S2: DYRK1B blockade facilitates PDAC cell proliferation.

A Western blot of *Dyrk1b* WT/KO cells showing the levels of DYRK1A/B protein. Shown is one representative blot of n=2. **B** Growth of WT/KO mKpc4 cells in soft agar (number of counted colonies present, n=1 performed in technical triplicate, mean ±SD). **C** Representative flow cytometry plots (related to figure 2D) of BrDU and propidium iodide (PI) labelling of mKpc4 cells. Left low population (violet) – cells in G1-phase; middle population (green) – BrDU-positive cells in S-phase; right low population (pink) – cells in G2-phase. **D** Representative flow cytometry plots (related to figure 2E) of mKPC4 cells treated with DMSO as solvent or 1 μM AZ191 and stained with anti-BrDU antibody and propidium iodide. Left low population – cells in G1-phase; middle population – BrDU-positive cells in S-phase; right low population – cells in G2-phase. **E** WB showing changes in mTOR, AKT and S6 phosphorylation in *Dyrk1b* WT/KO mKpc4 cells. Shown is one representative blot of n=2.

Figure S3: Transcriptomic changes in *Dyrk1b*-KO tumors.

A Tumor size changes over time (subcutaneous allograft growth in C57BL/6 mice). Animals received either *Dyrk1b*-WT (black curve) or KO (clone 2.7; red curve) mKpc4 cells on day 0. Shown is the mean ±SEM. **B** Downregulated gene signatures in *Dyrk1b*-KO tumors (vs *Dyrk1b*-WT tumors). **C** F4/80 IHC of WT/KO2.7 allograft tumors as depicted in panel A. Scale bar: 100 μm. **D** Myeloperoxidase (MPO) staining of tumor-associated neutrophils (TANs) in WT/KO tumor tissue. Human PDAC was included as positive control (the antibody recognizes mouse and human MPO, see e.g. [2]). Scale bar: Left/middle panel 100μm; right panel 200 μm. **E** Quantification of IF imaging of WT/KO5.3 allograft tumor depicting F4/80-TNF double-positive Mphs (M1 TAMs). Mean of several viewing areas from four animals each ±SD (1-tailed t-test). **F** F4/80-CD206 IF of WT and KO5.3 tumor tissue (M2 TAMs). Scale bar: 30 μm. **G**

Quantification of IF imaging as depicted in panel F. Mean of several viewing areas from four animals each ±SD (1-tailed t-test). **H-J** Macrophage marker gene expression (bulk RNAseq, in CPM) in WT/KO5.3 allograft tumors. Each dot represents one tumor (mean ±SD). **K** F4/80-Ki67 IF of WT and KO5.3 tumor tissue to assess proliferating Mphs. Scale bar: 30 μm. **L** Quantification of IF imaging as depicted in panel K. Mean of several viewing areas from five animals each ±SD (1-tailed t-test). **M** Quantification of pan-Cytokeratin (CK)/Ki67 IF imaging (not shown) to assess proliferating cancer cells. Mean of several viewing areas from five animals each ±SD (1-tailed t-test). **N** Flow cytometric determination of CD4/IFNγ double-positive T-cells in WT/KO5.3 allograft tumors. Each dot represents one tumor (mean ±SD). **O** Flow cytometric determination of CD4/TNF double-positive T-cells in WT/KO5.3 allograft tumors. Each dot represents one tumor (mean ±SD).

Figure S4: A *Dyrk1b*-controlled cancer cell secretome affects macrophage functions.

A-C Relative mRNA expression determined by qRT-PCR of M1-like (A-B) and M2-like (C) genes in mouse BMDM either untreated or stimulated with SN collected from WT or KO mKpc4 cells. Shown is one representative of n=3-6 measured in triplicate (mean ±SD). **D** Western blot depicting DYRK1B protein levels in Panc1 cells stably expressing a non-targeting control shRNA (shCon) or *DYRK1B*-targeting shRNA. The latter included the clones #9 (generated with sh*DYRK1B*_1) and #7 (generated with sh*DYRK1B*_3). Actin was used as loading control. Shown is one representative of n=2 western blots. **E** WB of cells in panel D depicting DYRK1A protein levels. Shown is one representative of n=2 western blots. **F** WB of cells in panel D depicting phosphorylated levels of mTOR, AKT and S6. Shown is one representative of n=2 western blots. **G-I** Relative mRNA expression determined by qRT-PCR of M1-like (G-H) and M2-like (I) genes in human PBMC-derived macrophages either untreated or stimulated with SN from control (shCon) or *DYRK1B*-KD clones #7 and #9. Shown is one representative of n=3 measured in triplicate (mean ±SD). **J** Migration of human PBMC-derived macrophages towards plain 0.5%-containing medium (no CM) or medium containing 50% of SN from control (shCon) Panc1 cells or from *DYRK1B*-KD clones #7 and #9. Shown is one representative of n=3 measured in triplicate wells (±SD).

Figure S5: DYRK1B-dependent impact of cancer cells on macrophage phagocytosis.

A Representative flow cytometry plots depicting the phagocytic capability of BMDM to engulf either WT or KO mKpc4 cells. BMDM are labelled in green, tumor cells are in deep red. **B** Relative phagocytosis of control (shCon) or *DYRK1B*-KD Panc1 cells by human PBMC-derived macrophages phagocyte as percentage of double-positive macrophages. Mean of n=3 ±SD. **C** Representative flow cytometry plots of data shown in B. Macrophages are labelled in green, and tumor cells are in deep red. **D** Relative

Supplemental material

BMJ Publishing Group Limited (BMJ) disclaims all liability and responsibility arising from any reliance placed on this supplemental material which has been supplied by the author(s)

Gut

phagocytic capability of BMDM to engulf mKpc4 cells treated with either DMSO or 1 µM AZ191 for 96 h. Results are presented as fold change in percentage of double-positive macrophages. Mean of n=5 ±SD. **E** Representative flow cytometry plots of data shown in D. Macrophages are labelled in green, and tumor cells are in deep red. **F** Relative phagocytic capability of human PBMC-derived macrophages to engulf Panc1 cells treated with either DMSO or 1 µM AZ191 and presented as fold change in percentage of double-positive macrophages. Mean of n=3 ±SD. **G** Representative flow cytometry plots of data shown in F. Macrophages are labelled in green, and tumor cells are in deep red. **H** Relative phagocytic capability of human PBMC-derived macrophages treated with conditioned media from either control (shCon) or *DYRK1B*-KD towards Panc1 cells. Shown is one representative of n=2 measured in triplicate (±SD) (Paired two-tailed t-test). **I** Representative flow cytometry plots of mean fluorescence intensity (MFI) of surface CD24 on WT and KO mKpc4 cells (relates to figure 5G). **J** Western blot depicting absolute CD24 protein levels in mKpc4 cells treated with DMSO or 1 µM AZ191 for 48 h. Actin was used as loading control. Shown is one representative blot of n=2. **K** Relative mean fluorescence intensity (MFI) of surface CD24 on mKpc4 cells treated either with DMSO or with 1 µM AZ191 for 96 h. Mean of n=3 ± SD. **L** Representative flow cytometry plots of mean fluorescence intensity (MFI) of surface CD24 on mKpc4 cells treated either with DMSO or with one of the following DYRK1B inhibitors: 1 µM AZ191, 1 µM Harmine, 1 µM Indy. Relates to Fig. S5K. **M** Relative mRNA expression of *Cd24* determined by qRT-PCR in mKpc4 cells treated either with DMSO or with 1 µM AZ191 for 48 h. Mean n=3 ±SD. **N** Representative flow cytometry plots of mean fluorescence index (MFI) of surface CD24 on control (shCon) Panc1 cells and *DYRK1B*-KD clones #7 and #9. Relates to figure 5L. **O** Relative mRNA expression of *CD24* determined by qRT-PCR in control (shCon) or *DYRK1B*-KD Panc1 cells. Mean of n=3 ±SD.

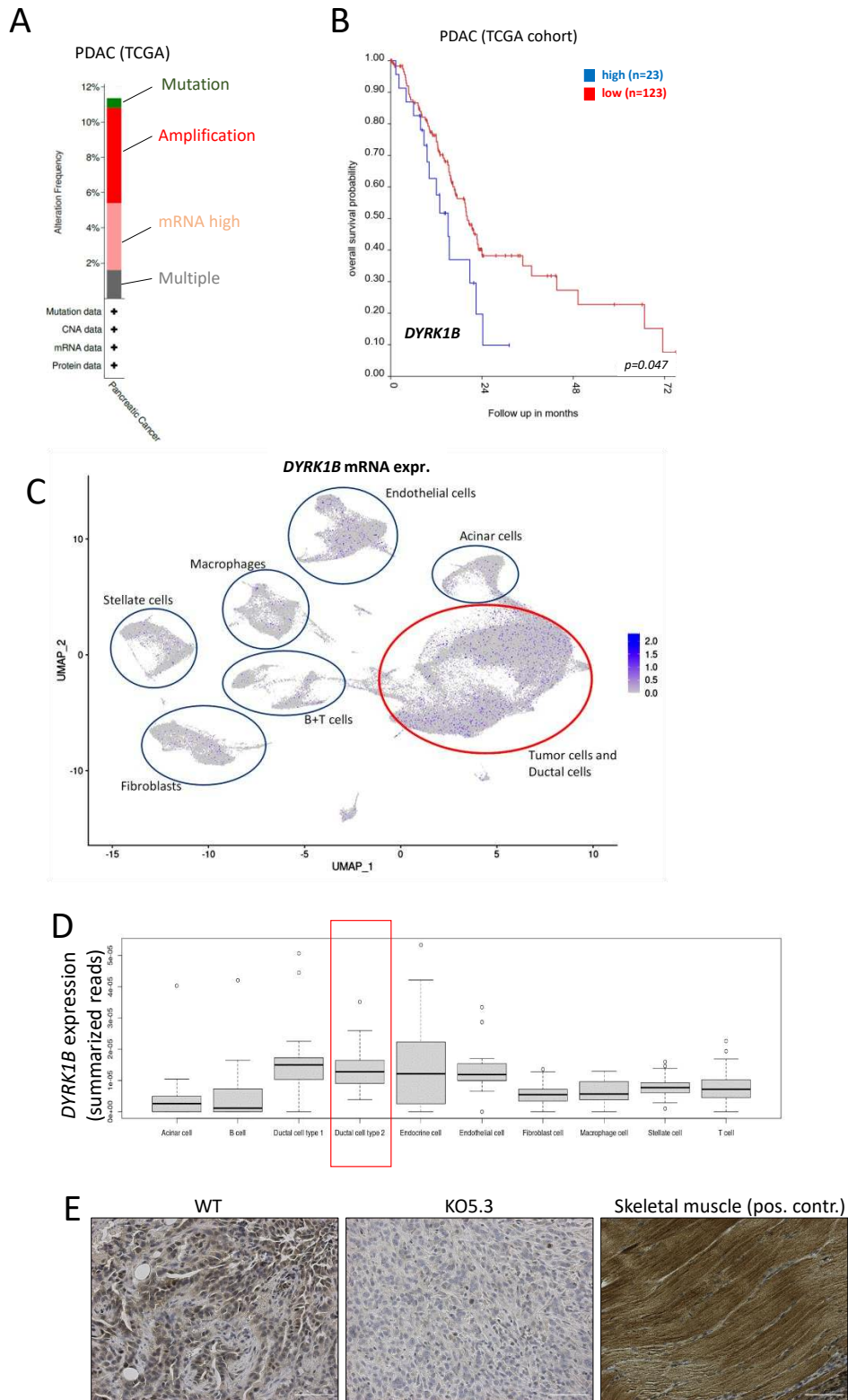**Figure S6: A DYRK1B-directed therapy extends survival in an autochthonous mouse model of PDAC.**
A. Kaplan-Meier overall survival curve of KPC mice treated with vehicle (black line, n=13) or with 70 mg/kg once weekly Gemcitabine (red line, n=6) (logrank test). **B** Kaplan-Meier overall survival curve of KPC mice treated with vehicle (black line, n=13) or with twice weekly 5 mg/kg AZ191 (red line, n=5). **C** F4/80 IHC of KPC animals treated with solvent or AZ191 (treated until humane endpoint). Scale bar: 100 µm. **D** Quantification of IHC as depicted in panel C. Each dot represents one tumor (mean ±SD). **E** Kaplan-Meier overall survival curve of KPC mice treated with solvent (black line, n=13) or with a combination of KU0063794 (KU; 5 mg/kg; twice weekly) and AZ191 (AZ; 5 mg/kg; twice weekly) (red line, n=5). **F** Kaplan-Meier overall survival curve of KPC mice treated with solvent (black line, n=13) or with a combination of Gemcitabine (70 mg/kg once weekly) plus AZ191 (5 mg/kg; twice weekly) (red line, n=3).

Supplemental material

BMJ Publishing Group Limited (BMJ) disclaims all liability and responsibility arising from any reliance placed on this supplemental material which has been supplied by the author(s)

Gut

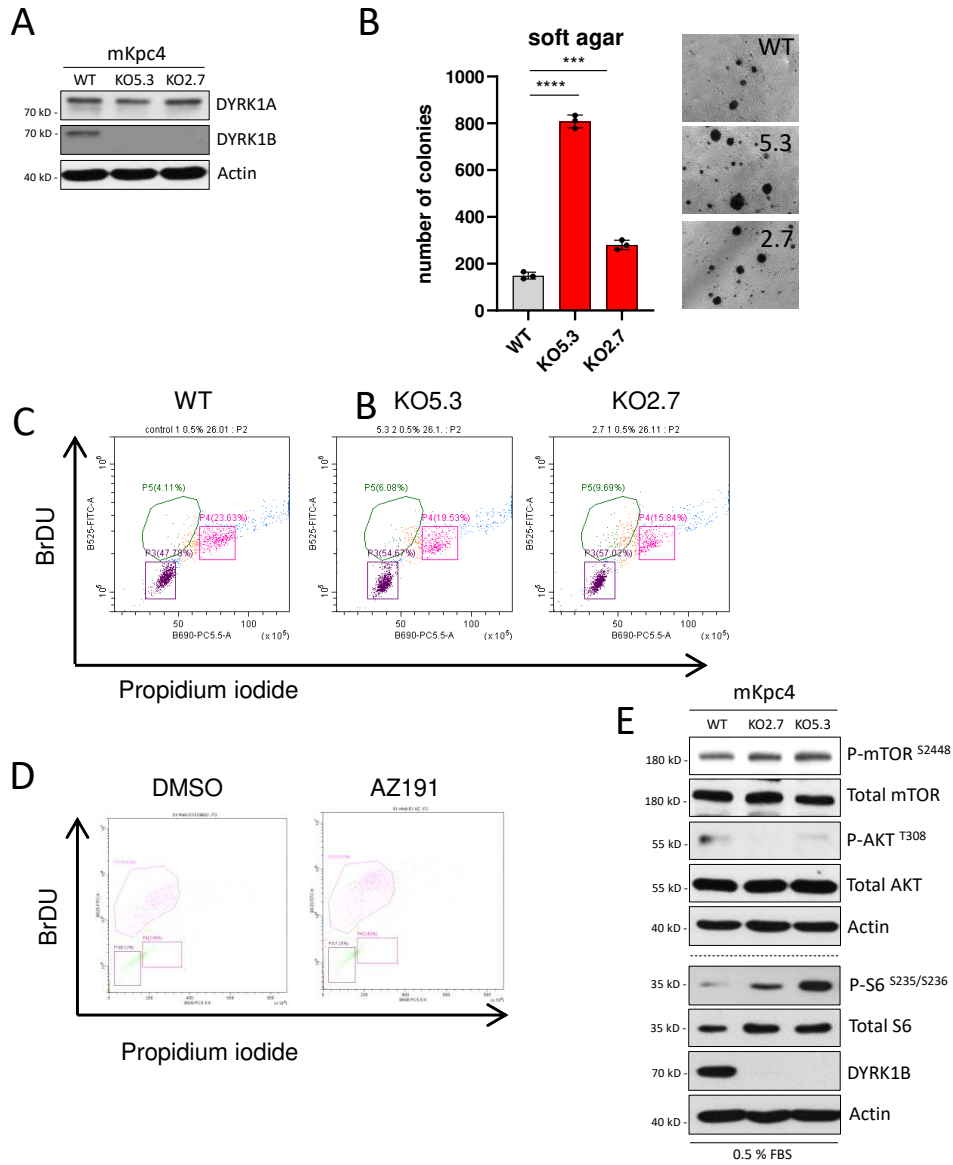**Figure S7: Intra-tumoral macrophage abundance correlates with DYRK1B levels in human PDAC patients.**

A Correlation between *CD86* and *DYRK1B* bulk mRNA expression in PDAC patients of the TCGA cohort. **B** Correlation between *HLA-DRA* and *DYRK1B* bulk mRNA expression in PDAC patients of the TCGA cohort. **C** Correlation between *MSR1* and *DYRK1B* bulk mRNA expression in PDAC patients of the Yang cohort [3]. **D** Correlation between *CD80* and *DYRK1B* bulk mRNA expression in PDAC patients of the Yang cohort. **E** Correlation between *CD86* and *DYRK1B* bulk mRNA expression in PDAC patients of the Yang cohort.
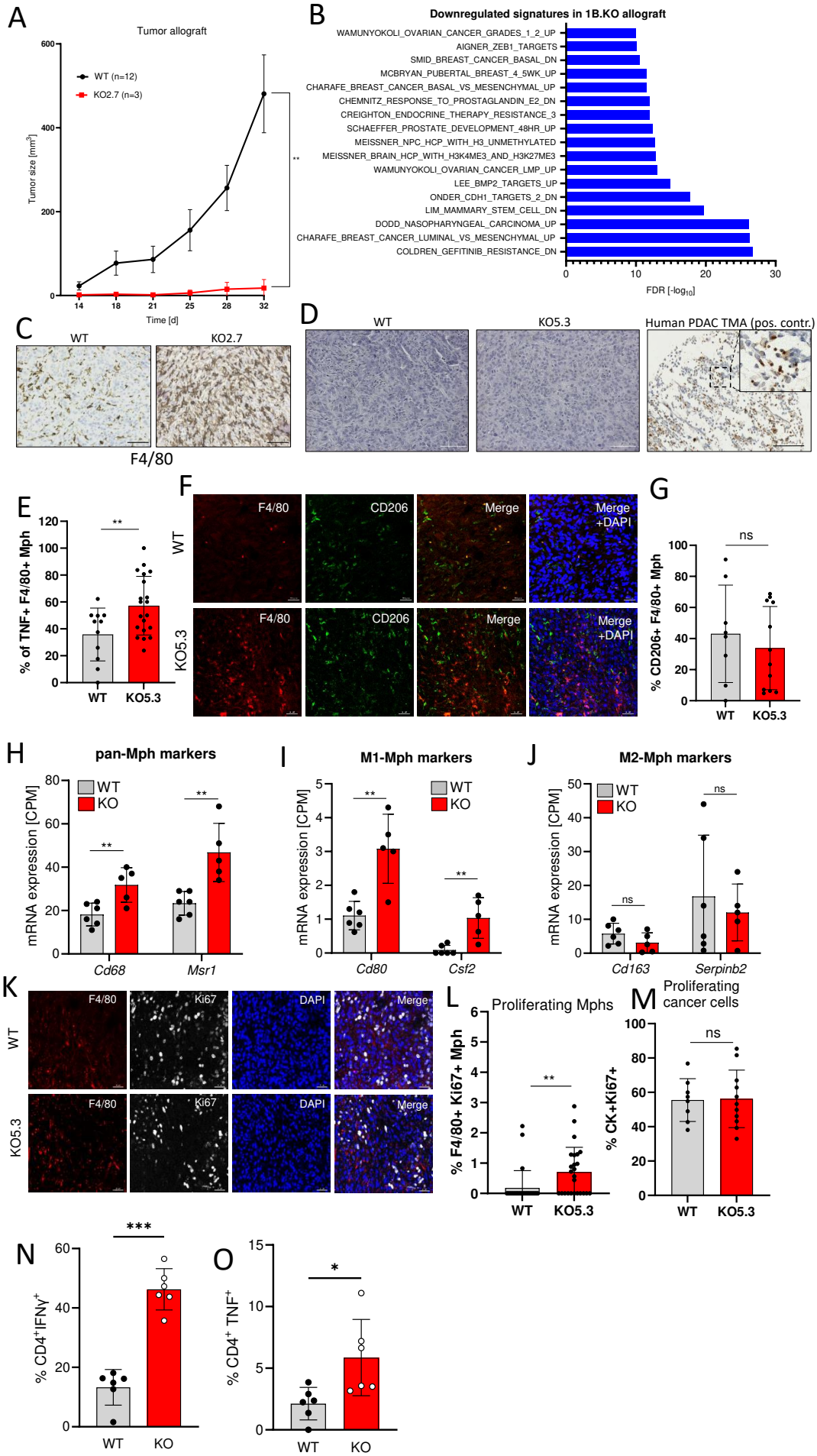
References

1. Peng, J.; Sun, B.-F.; Chen, C.-Y.; Zhou, J.-Y.; Chen, Y.-S.; Chen, H.; Liu, L.; Huang, D.; Jiang, J.; Cui, G.-S.; et al. Single-cell RNA-seq highlights intra-tumoral heterogeneity and malignant progression in pancreatic ductal adenocarcinoma. *Cell Res.* **2019**, *29*, 725–738, doi:10.1038/s41422-019-0195-y.
2. Awasthi, D.; Chopra, S.; Cho, B.A.; Emmanuelli, A.; Sandoval, T.A.; Hwang, S.-M.; Chae, C.-S.; Salvagno, C.; Tan, C.; Vasquez-Urbina, L.; et al. Inflammatory ER stress responses dictate the immunopathogenic progression of systemic candidiasis. *J. Clin. Invest.* **2023**, *133*.
3. Yang, S.; Tang, W.; Azizian, A.; Gaedcke, J.; Ströbel, P.; Wang, L.; Cawley, H.; Ohara, Y.; Valenzuela, P.; Zhang, L.; et al. Dysregulation of HNF1B/Clusterin axis enhances disease progression in a highly aggressive subset of pancreatic cancer patients. *Carcinogenesis* **2022**, *43*, 1198–1210, doi:10.1093/carcin/bgac092.
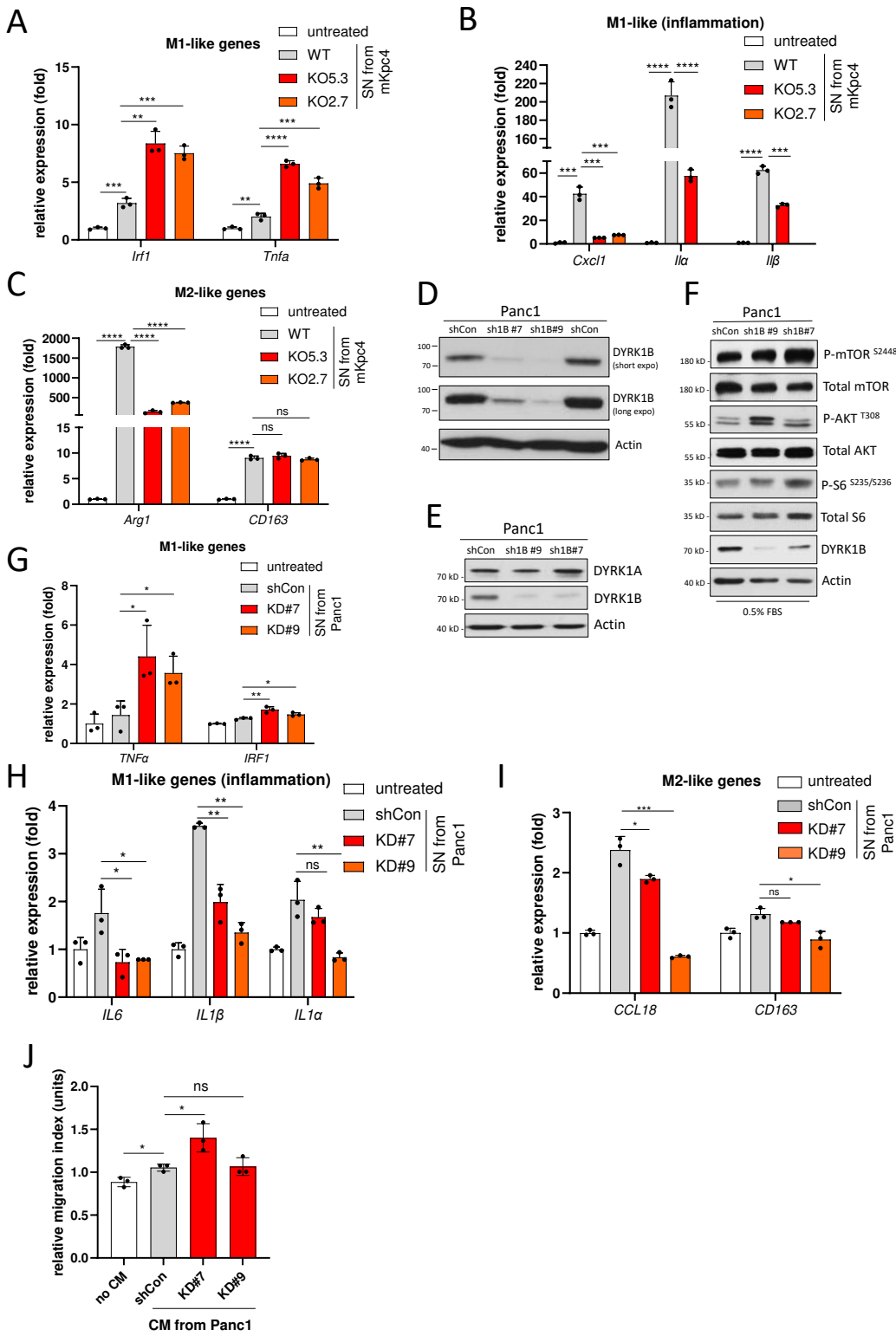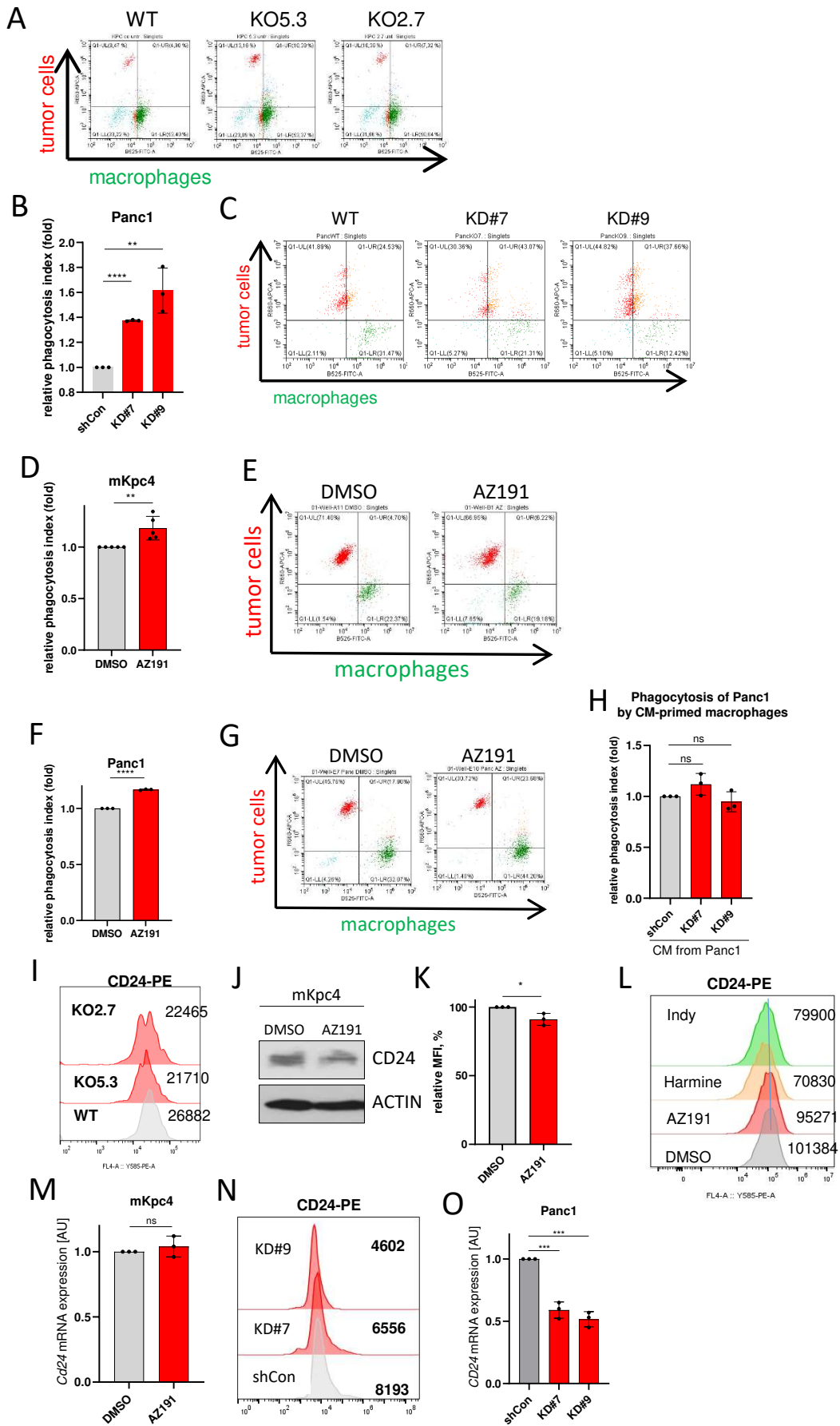
Supplemental material

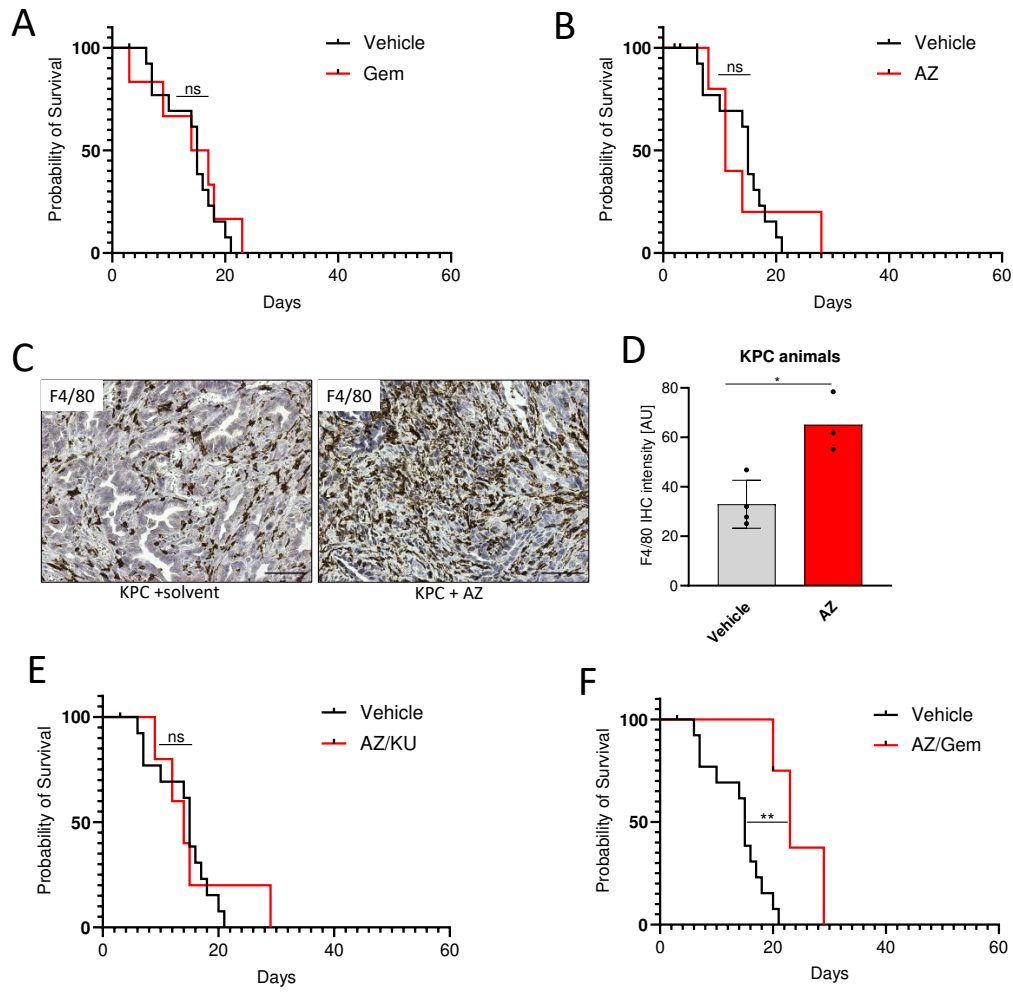BMJ Publishing Group Limited (BMJ) disclaims all liability and responsibility arising from any reliance placed on this supplemental material which has been supplied by the author(s)

Gut

- Figure S1 -

- Figure S2 -

Supplemental material

BMJ Publishing Group Limited (BMJ) disclaims all liability and responsibility arising from any reliance placed on this supplemental material which has been supplied by the author(s)

Gut

- Figure S3 -

Supplemental material

BMJ Publishing Group Limited (BMJ) disclaims all liability and responsibility arising from any reliance placed on this supplemental material which has been supplied by the author(s)

Gut
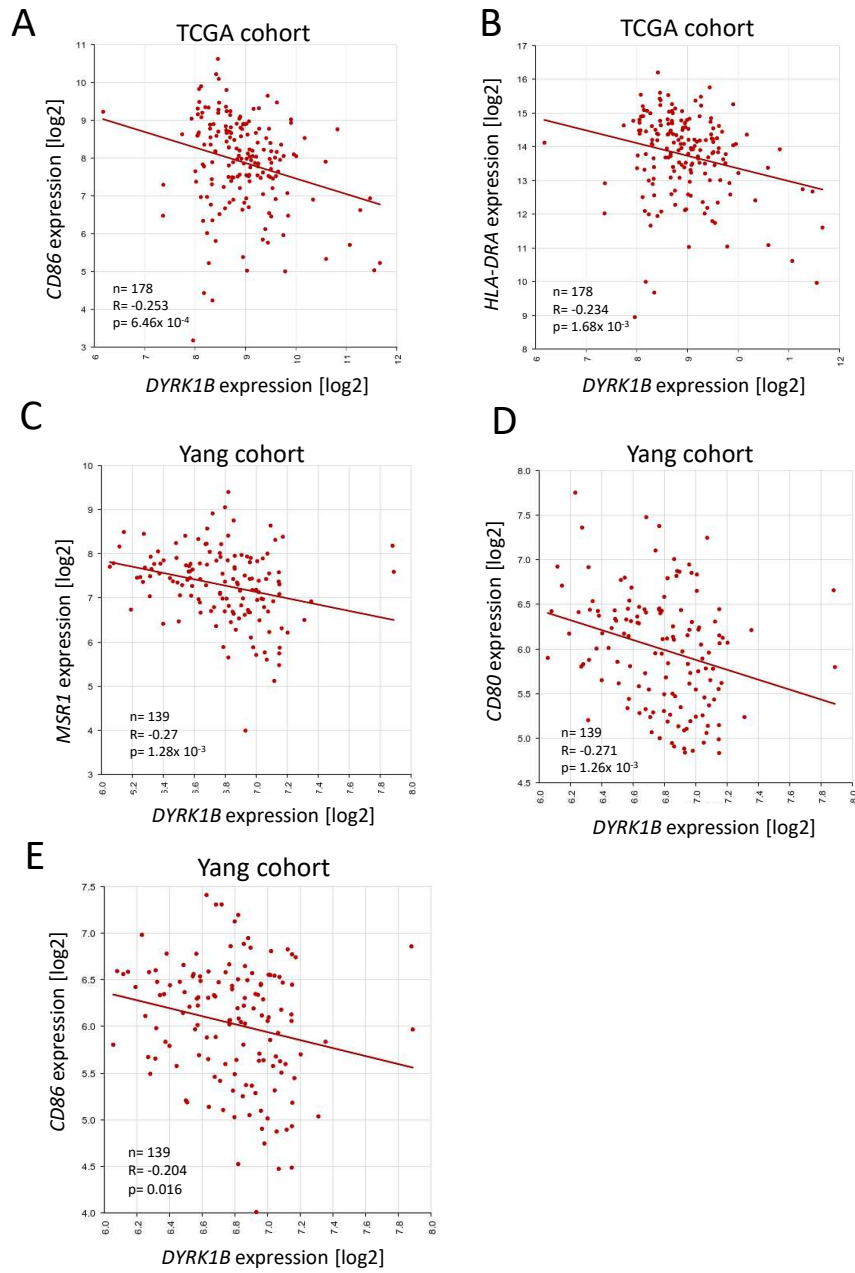

- Figure S4 -

- Figure S5 -

- Figure S6 -

- Figure S7 -

Supplemental materials

qRT-PCR primers

Murine primers (5'->3'):

mSaa1/2	CATGCTCGGGGGAACTATGATGCTG	CTGTTGGCTTCCTGGTCAGCAATGG
mSaa3	CATGCTCGGGGGAACTATGATGCTG	AAGTGGTTGGGGTCTTTGCCACTCC
mCxcl1	GAGGCTTGCCTTGACCCTGAAGCTC	GTCAGAAGCCAGCGTTCACCAGACA
mIL6	TCCTTCCTACCCCAATTTCCAATGCTC	GGATGGTCTTGGTCCTTAGCCACTCCT
mCsf3	TGGACTTGCTTCAGCTGGATGTTGC	AGGCAGAAGTGAAGGCTGGCATGG
mCol4a1	TCGCCACCATAGAGAGAAGCGAGATG	ACCATGTTGTGACGGTGGCAGAGG
mCol1a1	TGGCAAAGACGGACTCAACGGTCTC	GAAGTCATAACCGCCACTGGGAGGTC
mHas2	ACCCTATGGTTGGAGGTGTTGGAGGA	CACGCTGCTGAGGAAGGAGATCCAG
mActa2	CCTGGAGAAGAGCTACGAACTGCCTGA	TTTCGTGGATGCCCGCTGACTC
mPkp1	TGCTTCAGCAACAGGGGTGACAAGA	CATGAGGTTCAGGTAGGTCCGGATGG
mLif	GCAGCGCCAATGCTCTCTTCATTTC	GCGCACATAGCTTTTCCACGTTGTTG
mTgfb1	GCAGAGCTGCGCTTGCAGAGATTAAAA	ACTCAGGCGTATCAGTGGGGGTCAG
mTgfb2	TGAAAACCAGAGCGGAGGGTGAATG	CACGAAGGTACAGCAGGGGCAGTGT
mTgfb3	CTTCTGCTCAGGCCCTTGCCCATAC	ACGCCTCTGGGTTCAGGGTGTTGTA
mPai1	ATGGCCCCCACGGAGATGGTTATAG	CCATCACTTGGCCCATGAAGAGGAT
mCyr61	AGTGCGTCCTTGTGGACAACCAGTG	AGCCGCAGTATTTGGGCCGGTATTT
mGadd45a	GCTGAGCTGCTGCTACTGGAGAACGA	TAATCACGGGCACCCACTGATCCAT
mIrf1	CCAGGAACCAGAGGAAAGAGAGAAAG	CATGGCGACAGTGCTGGAGTC
mTnfα	GAAAGCATGATCCGGGACGTG	GATGGCAGAGAGGAGGTTGAC
mIl1a	AAGGAGAAGACCAGCCCGTGTTGC	ACCCGACTTTGTTCTTTGGTGGCAAT
mIl1b	GGCCTTGGGCCTCAAAGGAAAGAAT	TGCTGATGTACCAGTTGGGGAACTCTG
mArg1	CAAGACAGGGCTCCTTTCAG	GGCTTATGGTTACCCTCCCG
mCd163	GGCACTCTTGGTTTGTGGAG	GCCTTTGAATCCATCTCTTGG
mCd24	TGCTGCTTCTGGCACTGCTCCTACC	CCCCTCTGGTGGTAGCGTTACTTGGA
mP0	TGCACTCTCGCTTTCTGGAGGGTGT	AATGCAGATGGATCAGCCAGGAAGG

Supplemental material

BMJ Publishing Group Limited (BMJ) disclaims all liability and responsibility arising from any reliance placed on this supplemental material which has been supplied by the author(s)

Gut

Human primers (5'->3'):

|		
hTNFα	GAAAGCATGATCCGGGACGTG	GATGGCAGAGAGGAGGTTGAC
hIL6	AACTCCTTCTCCACAAGCGCC	GTGGGGCGGCTACATCTTT
hIRF1	CCAGAGAAAAGAAAGAAAGTCGAAGTCC	CATGGCGACAGTGCTGGAGTC
hIL1A	GCCCAAGATGAAGACCAACCAGTGC	TGCCGTGAGTTTCCCAGAAGAAGAGG
hIL1B	TGAAAGCTCTCCACCTCCAGGGACA	GAGGCCCAAGGCCACAGGTATTTTG
hCCL18	TGCTCCTGTGCACAAGTTGG	CTGGGGGCTGGTTTCAGAAT
hCD163	AATGGGAATTTATAACCCCAGTGAG	GGTGAATTTCTGCTCTCCATTCA
hCD24	CCAAGCACCCAGCATCCTGCTAGAC	GCATTAGTTGGATTTGGGGCCAACC
hP0	CCTTCTCCTTTGGGCTGGTCATCCA	CAGACACTGGCAACATTGCGGACAC

List of antibodies

| Antibody	Company	Order #	Application
DYRK1B	BioOrbyt	orb318969	IHC
DYRK1B	Cell Signaling Technology	#5672	WB
β-Actin	Sigma	A5441	WB
BrdU	Biozol	BLD-364104 (FITC)	Flow cytometry
αSMA	Cell Signaling Technology	19245	IHC
PDGFRβ	Cell Signaling Technology	3169	IHC
F4/80	Cell Signaling Technology	70076	IHC
Ki67	Abcam	ab15580	IHC
CD31	Cell Signaling Technology	77699	IHC
CD24	Abcam	ab290730 (mouse-spec.)	WB
CD24	BD Biosciences	555426, Clone ML5 (human-spec.)	WB
CD24 (PE)	Miltenyi	130-112-845 (human-spec.)	Flow cytometry
CD24 (PE)	Miltenyi	130-103-371 (mouse-spec.)	Flow cytometry
IgG (PE)	Miltenyi	130-113-438 (human)	Isotype control, Flow cytometry
IgG (PE)	Biolegend	400608 (mouse)	Isotype control, Flow cytometry
CD68	Dako/Agilent	M0876, Clone PG-M1	IHC
M-CSF	Biotechne/Novus	AF416-SP	Neutralizing Ab
CCL5	Biotechne/Novus	AF478-SP	Neutralizing Ab
CCL6	Biotechne/Novus	AF487-SP	Neutralizing Ab
CXCL2	Biotechne/Novus	AF452-SP	Neutralizing Ab
FcR Blocking	Miltenyi	130-059-901 (human-spec.)	Flow cytometry
Cd16/32 FcR blocking	Biolegend	101330 (mouse-spec.)	Flow cytometry
CD206 (Alexa 647)	Cell Signaling Technology	#43920	Tissue IF
F4/80 (Alexa 555)	Cell Signaling Technology	#99651	Tissue IF
Ki67 (Alexa 647)	Cell Signaling Technology	#12075	Tissue IF
Pan-Keratin (Alexa 488)	Cell Signaling Technology	#4523	Tissue IF
TNF-alpha	Biotechne	AF-410-NA	Tissue IF
F4/80 (APC)	Ebioscience	14-480-82	Flow cytometry
MHCII (APC-Cy7)	Biolegend	107628	Flow cytometry
CD206 (PerCP-Cy5.5)	Biolegend	141715	Flow cytometry
CD45 (VioBlue)	Miltenyi	130-110-802	Flow cytometry
CD4 (Brilliant violet)	Ebioscience	48-0041-82	Flow cytometry

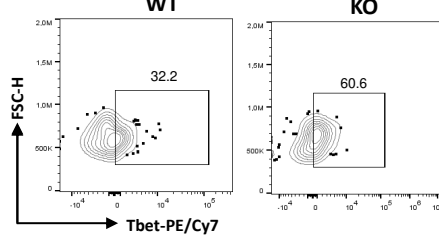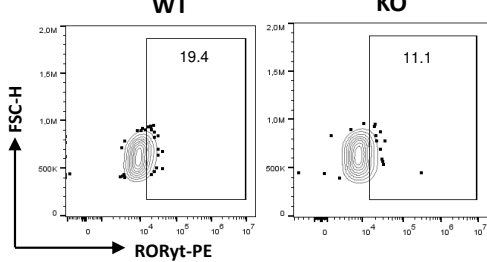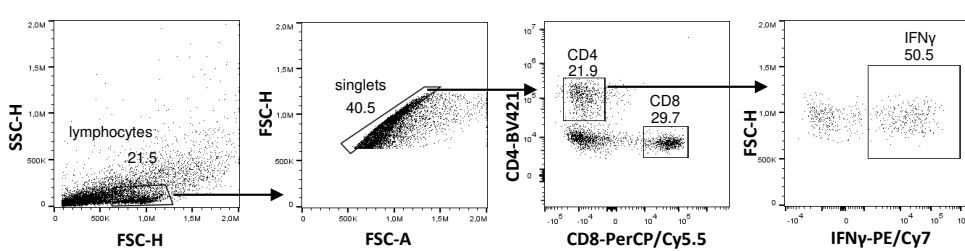|			
CD8 (PerCP-Cy5.5)	Biolegend	100732	Flow cytometry
IFNγ (PE-Cy7)	Biolegend	505826	Flow cytometry
TNF (FITC)	Ebioscience	11-7321-82	Flow cytometry
Tbet (PE-Cy7)	Biolegend	644824	Flow cytometry
RORγt	BD Bioscience	563081	Flow cytometry

Flow cytometry gating strategies

Total CD4⁺ or CD8⁺

IFNγ⁺
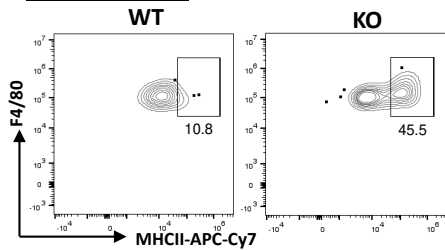

TNF⁺

Tbet⁺

RORγt⁺
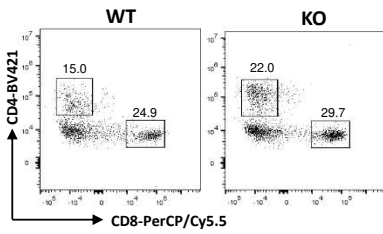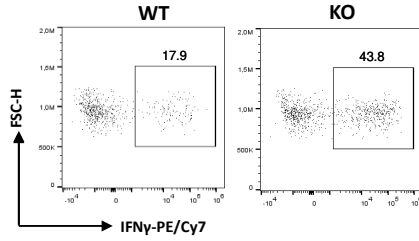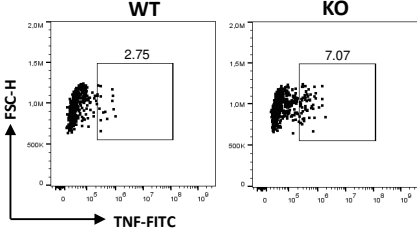
CD4⁺/IFNγ⁺

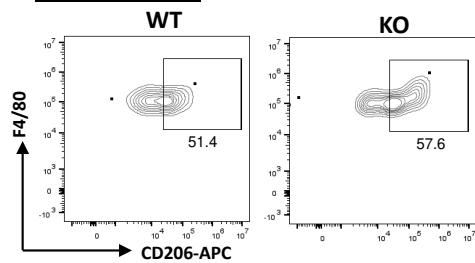**F4/80-MHCII⁺**

F4/80-CD206⁺

Reviewer access to submitted RNaseq data

RNAseq data has been deposited at BioStudies/Array Express and can be accessed via the following links:

- E-MTAB-13666 (*Dyrk1b* WT/KO in mKpc4 cells)

  https://www.ebi.ac.uk/biostudies/arrayexpress/studies/E-MTAB-13666?key=050421ec-ae16-4ad3-80b0-3b11f49a21ba

- E-MTAB-13667 (Mouse allograft with *Dyrk1b* WT/KO mKpc4 cells)

  https://www.ebi.ac.uk/biostudies/arrayexpress/studies/E-MTAB-13667?key=686b40d2-4f1c-4e29-bc1f-e62ce210e3b9

- E-MTAB-13668 (Mouse BMDMs treated with SN from *Dyrk1b* WT/KO mKpc4 cells)

  https://www.ebi.ac.uk/biostudies/arrayexpress/studies/E-MTAB-13668?key=62441f8c-e380-4613-85d8-84f9c27654d5